


RESEARCH

Open Access



Hydrogen peroxide induced by nerve injury promotes axon regeneration via connective tissue growth factor

Samuele Negro^{1,2†}, Fabio Lauria^{3†}, Marco Stazi^{1†}, Toma Tebaldi^{4,5}, Giorgia D'Este¹, Marco Pirazzini^{1,6}, Aram Megighian^{1,7}, Francesca Lessi⁸, Chiara M. Mazzanti⁸, Gabriele Sales⁹, Chiara Romualdi⁹, Silvia Fillo¹⁰, Florigio Lista¹⁰, James N. Sleigh^{11,12,13}, Andrew P. Tosolini^{11,12}, Giampietro Schiavo^{11,12,13}, Gabriella Viero³ and Michela Rigoni^{1,6*} 

Abstract

Regeneration of the neuromuscular junction (NMJ) leverages on extensive exchange of factors released from motor axon terminals (MATs), muscle fibers and perisynaptic Schwann cells (PSCs), among which hydrogen peroxide (H₂O₂) is a major pro-regenerative signal. To identify critical determinants of NMJ remodeling in response to injury, we performed temporal transcriptional profiling of NMJs from 2 month-old mice during MAT degeneration/regeneration, and cross-referenced the differentially expressed genes with those elicited by H₂O₂ in SCs. We identified an enrichment in extracellular matrix (ECM) transcripts, including *Connective Tissue Growth Factor (Ctgf)*, which is usually expressed during development. We discovered that Ctgf levels are increased in a Yes-associated protein (YAP)-dependent fashion in response to rapid, local H₂O₂ signaling generated by stressed mitochondria in the injured sciatic nerve, a finding highlighting the importance of signals triggered by mechanical force to motor nerve repair. Through sequestration of Ctgf or inactivation of H₂O₂, we delayed the recovery of neuromuscular function by impairing SC migration and, in turn, axon-oriented re-growth. These data indicate that H₂O₂ and its downstream effector Ctgf are pro-regenerative factors that enable axonal growth, and reveal a striking ECM remodeling process during nerve regeneration upon local H₂O₂ signaling. Our study identifies key transcriptomic changes at the regenerating NMJ, providing a rich source of pro-regenerative factors with potential for alleviating the consequences of peripheral nerve injuries.

Keywords: Connective tissue growth factor, Hydrogen peroxide, Nerve regeneration, Neuromuscular junction, Schwann cells, Yes-associated protein

Background

Peripheral nerves possess the capacity to regenerate after injury due to intrinsic properties of motor neurons (MNs) and a permissive local environment [1–4].

A complex and finely coordinated nerve injury response is orchestrated by a sequence of transcriptional events that involve the expression of specific sets of pro-survival and pro-regenerative genes [5], whose molecular triggers and mechanisms of action are only partially understood despite intense research. Regeneration of the neuromuscular junction (NMJ), which is the specialized synapse essential for motor function and survival, is the result of an intense cross talk between the motor axon terminal (MAT), perisynaptic Schwann cells (PSCs), muscle fibers,

[†]Samuele Negro, Fabio Lauria and Marco Stazi contributed equally to this work

*Correspondence: michela.rigoni@unipd.it

⁶ Myology Center (CIR-Myo), University of Padua, 35129 Padua, Italy
Full list of author information is available at the end of the article



and the basal lamina of the synaptic cleft [1, 6, 7]. This is the best characterized synapse due to its relative simplicity and experimental accessibility, which have facilitated the identification of molecules and mechanisms regulating its formation, maturation, maintenance, function, and regeneration [6–10]. The NMJ is a pathological target of several neurodegenerative diseases where cellular impairment begins prior to the appearance of clinical signs of disease [11–14]. Therefore, identification of additional factors and mechanisms driving synaptic dynamics and remodeling in response to injury holds great promise for a better understanding of the system, and the design of therapeutics able to counteract denervation and promote improved functional recovery.

As a starting point of the study, we unravelled the transcriptional changes that occur at the NMJ upon a rapidly reversible injury to the MAT. To do so, we choose to profile the transcriptome of NMJs in the mouse soleus: indeed, slow-twitch muscles (like the soleus) display a higher degree of plasticity and remodelling capability than fast-twitch muscles (e.g. the EDL) in response to denervation, and are less vulnerable to aging and neurodegenerative conditions [15–17]. We determined the transcriptional profiling of soleus NMJs during the time-course of nerve terminal degeneration and regeneration induced by the pore-forming toxin α -Latrotoxin (α -LTx). This neurotoxin specifically targets the MAT causing an acute, calcium-dependent degeneration that is fully reversible, with complete recovery within a few days in mice [18–20]. The process of MAT degeneration/regeneration by α -LTx is highly reproducible and can be temporally assessed by imaging the progressive disappearance/reappearance of pre-synaptic markers, and through quantitative electrophysiological analyses of neurotransmission [20, 21]. Upon damage, neurons produce hydrogen peroxide (H_2O_2), which acts as a major activator of Schwann cells (SCs) both in vivo and in vitro; this manifests as profound morphological changes that allow the clearing of nerve debris by phagocytosis, and the engagement of the pro-regenerative ERK pathway through phosphorylation [20, 22–24]. Therefore, to identify genes most critical to regeneration of the NMJ, we intersected the differentially expressed genes (DEGs) caused by α -LTx with our previously published data set of genes activated by H_2O_2 in SCs [23].

Among the top common hits, we identified the mRNA encoding the matricellular protein Connective Tissue Growth Factor (Ctgf), a component of the extracellular matrix (ECM) endowed with signaling function [25]. Ctgf is highly expressed during development and in dynamic processes, such as wound healing and cancer. Given that the role of Ctgf in nerve regeneration in mice had not been previously addressed, we investigated its expression,

localization, transcriptional regulation and contribution to recovery after toxin- and injury-induced NMJ damage.

Methods

Ethical statement

Eight to ten week-old CD1 mice were employed for laser capture microdissection (LCM) and transcriptional profiling, and for electrophysiological recordings. C57BL/6 mice expressing cytosolic GFP under the *plp* promoter [26] were kindly provided by Dr. W.B. Macklin (Aurora, Colorado), with the help of Dr. T. Misgeld (Munich, Germany), and used for imaging. The *proteolipid protein (plp)* gene promoter drives the expression of one of the major components of myelin predominantly in oligodendrocytes, SCs and the enteric glia of the gut, both in embryonic and postnatal tissues. Originally created to label oligodendrocytes in the central nervous system, the *plp*-GFP mice employed in the present study express cytoplasmic GFP in both myelinating and non-myelinating SCs of the peripheral nerves [26]. Mice expressing the Tomato protein specifically in ChAT (choline acetyltransferase)-positive neurons were obtained by crossing the C57BL/6 ChAT-Cre knock-in mice line with C57BL/6 Rosa26.tdTomato mice (Jackson Laboratories). C57BL/6 mice (8–12 weeks) were also used. Mice were maintained under a 12-h light/12-h dark cycle, and kept under constant temperature. Water and food were available ad libitum, and mice were fed with regular chow. All surgical procedures were performed under general anaesthesia (a cocktail of xilazine (48 mg/kg) and zoletil (16 mg/kg) via intraperitoneal injections or via isoflurane as reported in [27]). Paralysis was restricted to one hind limb, and did not impair food or water intake.

All experimental procedures involving animals and their care comply with the ARRIVE guidelines. Procedures carried out in Italy were approved by the ethical committee and by the animal welfare coordinator of the OPBA from the University of Padua. All procedures are specified in the projects approved by the Italian Ministry of Health, Ufficio VI (authorisation numbers: 359/2015 PR; 81/2017 PR; 521/2018 PR; 439/2019 PR) and were conducted in accordance with National laws and policies (D.L. n. 26, March 14, 2014), following the guidelines established by the European Community Council Directive (2010/63/EU) for the care and use of animals for scientific purposes. Animals were handled by specialised personnel under the control of inspectors from the Veterinary Service of the Local Sanitary Service (ASL 16-Padua), who are the local officers of the Ministry of Health.

Animal experiments in the United Kingdom were conducted in accordance with the European Community Council Directive of 24 November 1986 (86/609/EEC),

under license from the UK Home Office in accordance with the Animals (Scientific Procedures) Act 1986, and were approved by the UCL Institute of Neurology Ethical Review Committee.

Toxins and antibodies

α -LTx (LSP-130) and μ -conotoxin GIIIB (C-270) were purchased from Alomone. α -LTx purity was checked by SDS-PAGE, and its neurotoxicity by ex vivo mouse nerve-hemidiaphragm preparations, as previously described [28]. BoNT/A (Xeomin) was from Merz. All other reagents were from Sigma unless stated otherwise.

Antibodies and fluorescent conjugates with relative dilutions: α -BTx AlexaFluor555 (B35451 Thermo Fisher, 1:200), anti-Ctgf neutralizing antibody (70R-CR023 Fitzgerald, 2 μ g/40 μ l), anti-Ctgf for immunostaining (ab6992 Abcam, 1:200), anti-S100 (Z0311 Dako, 1:400), anti-GAP43 (ab75810 Abcam, 1:200), anti-NF (ab4680 Abcam, 1:800), anti-VAMP1 [29], anti-SNAP25 (ab24737 Abcam, 1:200), anti-SNAP-25 BoNT/A-cleaved [30], anti-syntaxin 1A/1B [31], anti-YAP (13008S, Cell Signaling, 1:200). Secondary AlexaFluor-conjugated antibodies (1:200) were from Thermo Fisher. A list of antibodies and the relative description is provided as Additional file 9.

Sample preparation and RNA extraction

Upon isoflurane anaesthetization, CD1 male mice of \approx 20 g were injected in the hind limb with α -LTx (5 μ g/kg in 15 μ l physiological saline, 0.9% NaCl + 0.2% gelatine) or vehicle (15 μ l saline). A few minutes before muscle collection, a local injection of fluorescent α -BTx was performed to visualize NMJs. At different time points (0, 4, 16, 72 and 168 h), treated mice (5 mice/group) were sacrificed by anaesthetic overdose (a cocktail of xilazine (48 mg/kg) and zoletil (16 mg/kg) via intraperitoneal injections) followed by cervical dislocation; soleus muscles were then rapidly collected, and frozen in liquid nitrogen-cooled isopentane. Cryo-sections (7–10 μ m thick) were transferred to UV-treated microscope glass slides. Microdissection was performed with a PALM RoboMover automatic laser microdissector (Carl Zeiss, Oberkochen, Germany). One hundred NMJs/sample were collected by LCM within 30 min, to preserve RNA integrity, and pooled. Total RNA was isolated by incubation with 50 μ l lysis buffer PKD (Qiagen) and 10 μ l proteinase K (Promega) at 55 $^{\circ}$ C overnight, with the sample upside down. The next day, samples were centrifuged for 10 min at 10,000 rpm, and RNA extracted using the Maxwell[®] 16 LEV RNA FFPE Purification Kit with automated system Maxwell 16 (Promega). RNA extraction was performed following the manufacturer's protocol starting from the DNase treatment step.

Library preparation

cDNA was obtained using the SMARTer Universal Low Input RNA kit (Clontech Laboratories), according to manufacturer's instructions. Libraries for RNA-Seq were obtained using the Nextera XT kit (Illumina) according to the manufacturer's guidelines. RNA sequencing was performed with NextSeq 500 (Illumina), loading a maximum of six, pooling libraries for each cartridge NextSeq High Output (300 cycles).

Computational analysis of sequencing data

One hundred bp paired-end reads were processed by removing Illumina Nextera adapters using Trimmomatic (v0.36). Processed reads were aligned to the mouse genome (GRCm38.p6) with STAR (v020201), using the Gencode M17 gene annotation, based on ENSEMBL release 92. Read duplicates were removed with Picard Tools MarkDuplicates (v2.18.9). All programs were used with default settings unless otherwise specified.

Multidimensional scaling (MDS) was performed with the *cmdscale* function of the "stats" package in R [32]. The analysis was based on the scaled expression values of 10,956 genes, determined at each time point, averaging the signals from replicates. The Euclidean distance was used as the distance metric in the analysis in Fig. 1B.

Gene expression levels were normalized among replicates using the TMM method implemented in the edgeR Bioconductor package [33]. Differentially expressed genes were detected using edgeR with a double threshold on the log₂-fold change (absolute value > 0.75), and the correspondent statistical significance ($P < 0.05$). Functional annotation of gene lists and enrichment analysis with Gene Ontology terms and KEGG pathways were performed with the clusterProfiler Bioconductor package.

Differentially-expressed genes resulting from H₂O₂ treatment in *R. norvegicus* were from [23]. Paralogous *M. musculus* genes were retrieved from ENSEMBL (release 92). Common up- and down-regulated genes in the two data sets were defined as the intersection of genes up- or down-regulated in at least one of the four time points of α -LTx treatment (4, 16, 72 and 168 h), and in at least one of the two time points upon H₂O₂ treatment (20 and 40 min).

Droplet digital PCR

Droplet digital PCR (ddPCR) was carried out using the ddPCRTM Supermix for Probes (No dUTP), the QX200TM Droplet Generator, the QX200 Droplet Reader, the C1000 TouchTM Thermal Cycler and the PX1TM PCR Plate Sealer (BIO-RAD, Hercules, California, USA) following the manufacturer's instructions.

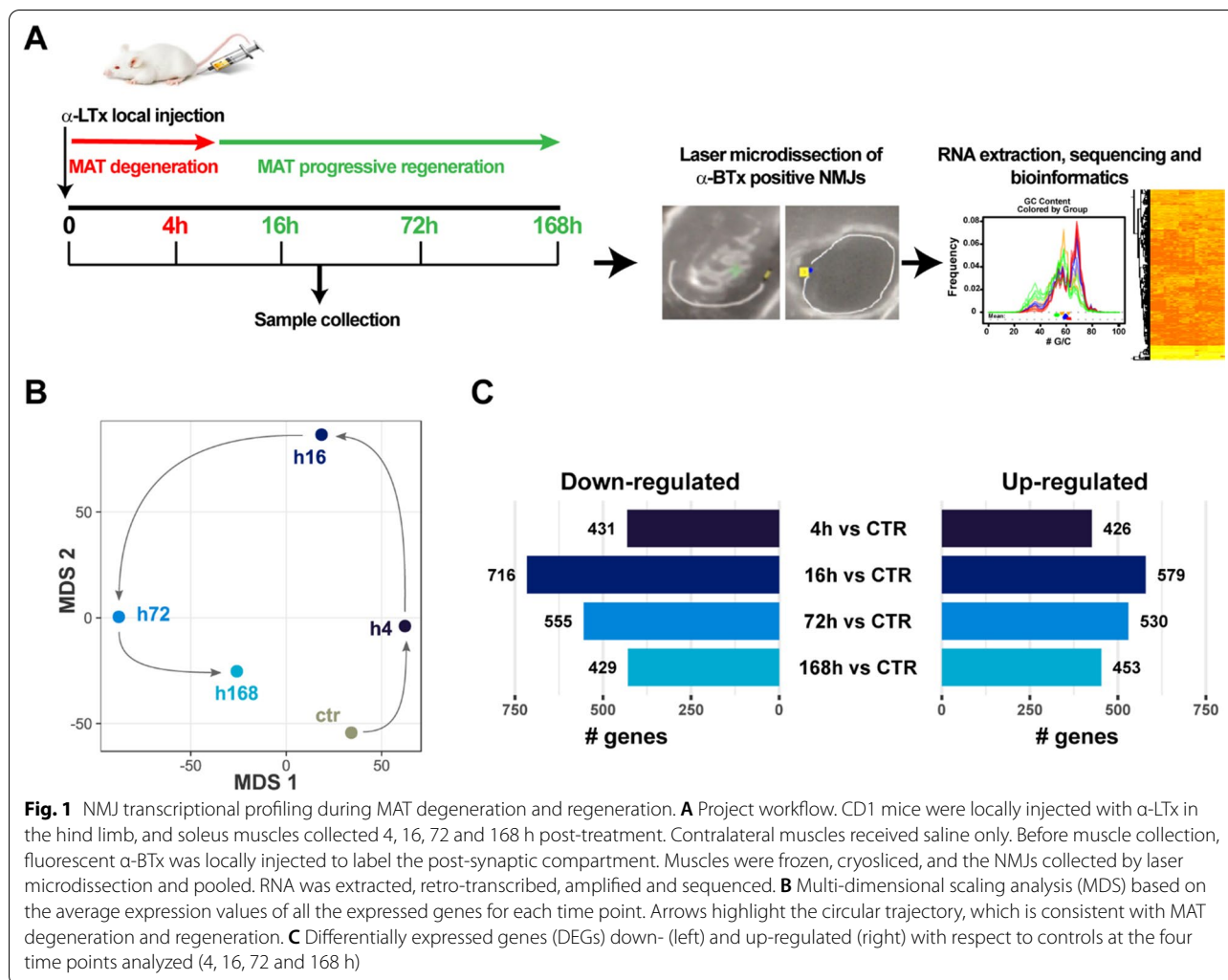


Fig. 1 NMJ transcriptional profiling during MAT degeneration and regeneration. **A** Project workflow. CD1 mice were locally injected with α-LTx in the hind limb, and soleus muscles collected 4, 16, 72 and 168 h post-treatment. Contralateral muscles received saline only. Before muscle collection, fluorescent α-BTx was locally injected to label the post-synaptic compartment. Muscles were frozen, cryosliced, and the NMJs collected by laser microdissection and pooled. RNA was extracted, retro-transcribed, amplified and sequenced. **B** Multi-dimensional scaling analysis (MDS) based on the average expression values of all the expressed genes for each time point. Arrows highlight the circular trajectory, which is consistent with MAT degeneration and regeneration. **C** Differentially expressed genes (DEGs) down- (left) and up-regulated (right) with respect to controls at the four time points analyzed (4, 16, 72 and 168 h)

Reactions were performed in triplicate in a 96 well plate using 10 μL/reaction of 2 × ddPCR Supermix for Probes (No dUTP), 1 μL/reaction of 20 × target primers/probe (FAM or HEX, BIO-RAD), 1 μL/reaction 20x reference primers/probe (FAM or HEX, BIO-RAD), 3 μL cDNA and 5 μL H₂O. Detection of Ctgf and Gapdh by ddPCR was performed using the following PrimePCR™ ddPCR™ Expression Probe Assay designed by BIO-RAD: CTGF-FAM (ID: qMmuCEP0053713) and GAPDH-HEX (ID: dMmuCPE5195283, BIO-RAD). All steps used a ramp rate of 2 °C/s. Results were analyzed in the QX200 Droplet Reader, the RNA targets were quantified using the QuantaSoft™ Software (BIO-RAD), and results were normalized to the control.

Electrophysiological recordings of evoked junctional potentials (EJPs)

EJPs were intracellularly recorded in vitro from single soleus muscle fibers following NMJ poisoning by α-LTx.

Anaesthetized mice were locally injected with α-LTx (5 μg/kg in 15 μL of 0.9% NaCl, 0.2% gelatin) in the hind limb [20, 21]. In a group of animals, after the local injection of the toxin, 2 μg of anti-Ctgf neutralizing antibody (in 40 μl physiological solution plus 0.2% gelatine) were intraperitoneally injected to induce the biochemical knockout of the molecule [21, 34], which begins rapidly after antibody injection and lasts for a long time, as the half-life of murine IgG antibodies exceeds 11 days [35]. 96 h later, when 50% neurotransmission blockade by the toxin is achieved (a value very suitable for assessing the impact of a treatment on nerve recovery of function), mice were sacrificed by cervical dislocation, and soleus muscles quickly excised and pinned to a Sylgard-coated petri dish (Sylgard 184, Down Corning USA). Recordings were performed in oxygenated Krebs–Ringer solution using intracellular glass microelectrodes (1.5 mm outer diameter, 1.0 mm inner diameter, 15–20 MΩ tip resistance; GB150TE, Science Products GmbH Germany),

filled with a 1:2 solution of 3 M KCl and 3 M CH₃COOK. Evoked neurotransmitter release was recorded in current-clamp mode, and resting membrane potential was adjusted with current injection to -70 mV. EJPs were elicited by supramaximal nerve stimulation at 0.5 Hz using a suction glass microelectrode (GB150TF, Science Products GmbH Germany) connected to a S88 stimulator (Grass, USA). Muscle fiber contraction during intracellular recordings was blocked by adding 1 μM μ-conotoxin. Intracellularly recorded signals were amplified with an intracellular amplifier (BA-01X, NPI, Germany), digitized using a digital A/C interface (NI PCI-6221, National Instruments, USA), and then fed to a computer for both on-line visualization and off-line analysis using appropriate software (WinEDR, Strathclyde University; pClamp, Axon, USA). Stored data were analyzed off-line using the software pClamp (Axon, USA).

Sciatic nerve compression/transection

The sciatic nerve was exposed at the level of the sciatic notch under general anaesthesia without damaging the gluteal musculature. Nerve compression (crush) was performed using haemostatic forceps, pre-dipped in powdered charcoal, to mark the crush site, by pinching the nerve 0.5 cm from the hip insertion for 20 s at the 3rd click of the haemostatic forceps. Transection of the sciatic nerve was performed using surgical scissor, leaving the edge juxtaposed [36]. The gluteal musculature was re-opposed and the skin sutured using 6–0 braided silk, non-absorbable sutures (ETHLCON2 biological instruments, 8697).

After surgery, mice were intraperitoneally injected once a week with anti-Ctgf antibodies (2 μg in 40 μl physiological solution plus 0.2% gelatine) or vehicle [34, 37], and electrophysiological measurements (in the case of crush) and immunofluorescence (crush and cut) were performed at different time points after injury.

In selected experiments, after sciatic nerve exposure, but before nerve compression, catalase (C1345, Sigma Aldrich) was intra-sciatically injected (1 mM in physiological solution, 2 μl injection volume) using a pulled graduated glass micropipette, gently inserted in the medial area of the sciatic nerve under the perineurium [38].

Electrophysiological recordings of compound muscle action potentials (CMAPs)

CMAPs were recorded from mice 18 or 28 days following sciatic nerve crush [37, 39, 40]. The 28 d time-point corresponds to 50–60% neurotransmission recovery following nerve compression, a value that is very suitable for assessing the impact of a treatment on nerve recovery of function [37]. Upon general anaesthesia,

the sciatic nerve was exposed at the sciatic notch, and a small piece of parafilm was slid under the nerve, which was kept moist with phosphate buffered saline (PBS). A pair of stimulating needle electrodes (Grass, USA) were then advanced until gently touching the exposed sciatic nerve, above the site of crush lesion, using a mechanical micromanipulator (MM33, FST, Germany). A pair of electromyography needle electrodes (Grass, USA) were used for electromyographic recording of gastrocnemius muscle fibre activity. The recording needle electrode was inserted halfway into the gastrocnemius muscle, while the indifferent needle electrode was inserted in the distal tendon of the muscle. CMAPs were recorded following supramaximal stimulation of the sciatic nerve at 0.5 Hz (0.4 ms stimulus duration) using a stimulator (S88, Grass, USA) via a stimulus isolation unit (SIU5, Grass, USA) in a capacitance coupling mode. To reach supramaximal stimuli (5–15 mV for controls, up to 50 mV after nerve damage), the sciatic nerve was stimulated with increasingly intense stimuli until the CMAP value ceased to increase. Recorded signals were amplified by an extracellular amplifier (P6 Grass, USA), digitized using a digital A/C interface (National Instruments, USA), and then fed to a computer for both on-line visualization and off-line analysis using appropriate software (WinEDR, Strathclyde University; pClamp, Axon, USA). Stored data were analyzed off-line using pClamp software (Axon, USA).

Immunohistochemistry

Soleus muscles were dissected at different time points after local administration of α-LTx, or 21 days after BoNT/A (0.5 U in 25 μl physiological solution plus 0.2% gelatin), w/wo treatment with anti-Ctgf neutralizing antibodies, then fixed in 4% PFA in PBS for 30 min at RT, and quenched in 0.24% NH₄Cl PBS for 20 min. After permeabilization and 2 h saturation in blocking solution (15% goat serum, 2% BSA, 0.25% gelatine, 0.20% glycine, 0.5% Triton-X100 in PBS), samples were incubated with primary antibody against syntaxin 1A/1B for 72 h in blocking solution at 4 °C. Muscles were then washed, and incubated with secondary antibodies and α-BTx AlexaFluor-555 to stain post-synaptic acetylcholine receptors (AChRs). Images were collected with a Leica SP5 confocal microscope equipped with a 40× and 63× HCX PL APO NA 1.4 oil immersion objective. Laser excitation line, power intensity and emission range were chosen according to each fluorophore in different samples to minimize bleed-through. Orthogonal projection and 3D analysis were performed with ImageJ software (*Orthogonal views* command in *Image-Stacks* section and 3D viewer plugin). The orthogonal projection method was used with a stack to display the XZ and YZ planes at a given point in the 3D image.

Pseudocolor image analysis: the 8 bit image format, acquired by confocal microscope, is associated with a signal intensity gradient (LUT) in grayscale, with pixel intensity values ranging from highest to lowest intensity. The grayscale image is converted in pseudocolors by Fiji imaging software, by assigning colors to the gray levels (pseudocolor Fire). The pseudocolor scale is added in the corresponding figure. White corresponds to the highest intensity, black to the lowest. This colored image, when displayed, allows an easier identification of certain features by the observer.

Sciatic nerves were isolated at different time points following crush or cut, w/wo treatment with anti-Ctgf neutralizing antibodies, fixed in 4% PFA in PBS for 30 min, sucrose-cryoprotected overnight, and embedded in OCT. Samples were slowly frozen in isopentane cooled with liquid nitrogen vapours, and cryo-sliced (20 μ m thickness) using a Leica CM1520 cryostat. Slices were processed for immunostaining as described in [37]. In some experiments, whole mount staining of the nerve was performed as described in [41].

Imaging of H₂O₂ in the murine sciatic nerve

Live imaging experiments were performed in C57BL/6 mice following the protocol described in [27]. Briefly, after anaesthesia was initiated and maintained using isoflurane, the fur on the dorsal hind limb (ankle to hip) was shaved off, and mice were placed on a heat-pad for the duration of surgery. An incision was made in the trochanteric region and the skin covering the entire surface was removed, along with the biceps femoris muscle to expose the underlying sciatic nerve. The connective tissue underneath the sciatic nerve was gently disrupted using curved forceps to enable the placement of a small piece of parafilm aiding the subsequent imaging. Once the sciatic nerve was exposed, 1 mM PF6-AM (A14086 AdooQ Bioscience) in 2 μ l saline was injected into the nerve. Peroxyfluor-6 acetoxymethyl ester (PF6-AM) is a chemoselective fluorescent indicator for H₂O₂. The molecule features a boronate chemical switch that allows for selective detection of H₂O₂ over other ROS, combined with acetoxymethylester (AM) protected phenol and carboxylic acid groups for enhanced cellular retention and sensitivity [42]. The anaesthetised mouse was then transferred to an inverted LSM780 laser scanning microscope (Zeiss) equipped within an environmental chamber pre-warmed and maintained at 37 °C. Using a 10x, Plan-Apochromat 10x/0.3 M27 (Zeiss), sciatic nerves were imaged, before and after injury, with a frame acquisition rate consistent across comparable data sets. Injury was performed by the compression of the sciatic nerve, in the distal part, for 30 s with a flat handle micro jewellers forceps. One millimolar H₂O₂ was added directly

above the sciatic nerve by drops (total volume 20 μ l) at the end of the recordings as a positive control. The mitochondria-targeted antioxidant MitoTEMPO (SML0737, Sigma-Aldrich) or the NOX inhibitor VAS2870 (492,000 Calbiochem) were applied (1 mM) in the same way before injury. Imaging was completed within 20 min of anaesthesia. A minimum of three sciatic nerves were imaged per condition. Mean fluorescence was measured by averaging the intensity across the visible sciatic nerve area.

Primary cell cultures and treatments

Primary cultures of SCs and of spinal cord motor neurons (SCMNs), and the relative co-cultures, were prepared as previously described [20, 43]. Primary SCs were exposed to 50 μ M H₂O₂ in Krebs Ringer Buffer (KRH: HEPES-Na 25 mM at pH 7.4, NaCl 124 mM, KCl 5 mM, MgSO₄ 1.25 mM, CaCl₂ 1.25 mM, KH₂PO₄ 1.25 mM, glucose 8 mM) for different amounts of time at 37 °C, and then processed for immunofluorescence or ELISA.

Co-cultures between SCs and SCMNs were kept for 2–3 days in SCMNs medium before treatment, then exposed for different times to α -LTx (0.1 nM) in E4 medium (120 mM NaCl, 3 mM KCl, 2 mM MgSO₄, 2 mM CaCl₂, 10 mM glucose, and 10 mM HEPES-Na, pH 7.4) at 37 °C, and processed for immunofluorescence.

Immunofluorescence

Samples were exposed to H₂O₂ with or without the Transcriptional enhancer factor domain (TEAD) inhibitor VT107 (HY-134957 MedChemexpress, 10 μ M final concentration). VT107 is a potent inhibitor of TEAD4 palmitoylation [44]. All TEAD homologues require auto-palmitoylation on the sulfhydryl of a conserved cysteine to become functional. Samples were then fixed for 15 min in 4% PFA in PBS, quenched (0.24% NH₄Cl in PBS), permeabilized with 0.3% Triton X100 in PBS for 5 min at RT, and saturated with 3% goat serum in PBS for 1 h. After incubation with primary antibodies diluted in 3% goat serum in PBS overnight at 4 °C, samples were washed and then incubated with the corresponding AlexaFluor-conjugated secondary antibodies for 1 h at RT. Coverslips were mounted in Mowiol and examined by confocal (Leica SP5) microscopy. Fluorescence intensity was quantified using Fiji Software. Images were acquired using non-saturating settings, and the same imaging parameters were used for all samples.

ELISA

Ctgf was quantified in the supernatant of primary SCs cultured in 24-well plates and exposed for different time periods to 50 μ M H₂O₂. Briefly, the supernatant was collected and centrifuged at 12,000 \times g at 4 °C to eliminate

cell debris. Aliquots were immediately assayed according to manufacturer's instructions (PeproTech 900-M317). Ctgf standards were used in the range of 4 to 4000 pg/ml.

***In vitro* scratch wounding assay**

SCs were seeded onto 35 mm Glass Bottom Dishes (Mattek) on a coating of laminin (3 µg/ml) w/wo 100 ng/ml of recombinant human Ctgf (rCtgf, 120–19 Peprotech). Once fully confluent, the monolayers were scratched using a sterile 200 µl pipette tip following the protocol described in [45]. Monolayers were then gently washed twice with DMEM to remove cell debris, and incubated at 37 °C (5% CO₂ air atmosphere). Images were acquired 0, 8 and 24 h later. The wound scratch area was measured using ImageJ.

Statistical analysis

Sample size was determined based on data collected in our previously published studies. We used at least N=4 mice/group for electrophysiological analysis. For imaging and cell cultures studies, at least three independent replicates were performed. Mice were randomly allocated to the different treatment groups by the investigator. We ensured blinded conduct of experiments. For imaging analysis, the quantitation was conducted by an observer who was blind to the experimental groups. No samples or animals were excluded from the analysis. Data displayed in histograms are expressed as means ± SD. GraphPad Prism software was used for all statistical analyses except for RNAseq data, where the glmQLFTest function, which applies a quasi-likelihood F-test, was employed. Statistical significance was evaluated using unpaired Student's *t*-test, or paired Student's *t*-test for live-imaging experiments. Data were considered statistically different when **p* < 0.05, ***p* < 0.01, ****p* < 0.001.

Results

Nerve injury induces upregulation of ECM components at the regenerating NMJ

To profile the NMJ transcriptome during α-LTx-induced degeneration and the subsequent recovery, we injected the hind limb of mice with the toxin, and collected soleus muscles 4, 16, 72 and 168 h post-treatment. Contralateral, control muscles received saline only. These time points encapsulate the period of MAT degeneration and regeneration in soleus muscles as determined by immunostaining of the pre-synaptic marker Synaptosomal-Associated Protein, 25 kDa (SNAP25) and neurofilaments (NF) (Additional file 1: Fig. S1): 4 h (MAT degeneration with active phagocytosis by PSCs), 16 h (clearance of neuronal debris almost complete), 72 h (ongoing MAT re-growth), and 168 h

(morphological recovery) [20]. To visualise endplates, fluorescent α-BTx was bilaterally injected into soleus muscles prior to their dissection and rapid freezing. Sections were then cut, and one hundred NMJs/sample were collected by LCM, and processed for sequencing (Fig. 1A).

To understand the global changes occurring during MAT degeneration and regeneration, transcriptional states were first investigated by multi-dimensional scaling analysis (MDS), which summarises the similarity between each time point, based on the levels of all expressed genes. Notably, the degeneration and regeneration cycle is captured by the dynamic changes in NMJ transcriptomes, resulting in a ring-shaped configuration, where chronological stages follow a circular trajectory (Fig. 1B). Whilst the regeneration profile at 72 h is clearly distinct from that of a mature resting NMJ, at later stage of regeneration the transcriptome profile is approaching that of the pre-injury control state. This trend is consistent with the time-course of MAT degeneration and regeneration (Additional file 1: Fig. S1), and is further supported by the number of differentially expressed genes (DEGs) identified at the different time points (Fig. 1C, and Additional file 2). Differential expression analysis shows that the largest transcriptional variations occur between the 16 and 72 h time points, when the NMJ undergoes major morphological transformation (*i.e.*, phagocytosis of terminal debris by PSCs, axonal elongation, re-establishment of synaptic contacts). At the last time point analysed, the number of DEGs decreases, reflecting the anatomical recovery of the MAT.

Gene ontology and REACTOME pathway enrichment analyses reveal that genes largely related to metabolism and muscle development are downregulated, while genes involved in ECM homeostasis display a global increment (Additional file 1: Fig. S2 and Additional file 3). Among the latter, both regulatory members of the ECM (*e.g.*, the matricellular proteins tenascin C, thrombospondins, Ctgf, osteopontin, periostin, Wisp 1 and Wisp 2) and structural components (*e.g.*, different collagen isoforms) show an overall increase during regeneration. At variance from signalling members of the ECM, whose levels approach the baseline at the latest time point (168 h), the increment of collagens is kept high for a longer time (Additional file 1: Fig. S3A, B).

Thus, a striking remodelling of the ECM occurs during NMJ degeneration and recovery to support PSC activation, axonal re-growth and, ultimately, rescue of neurotransmission.

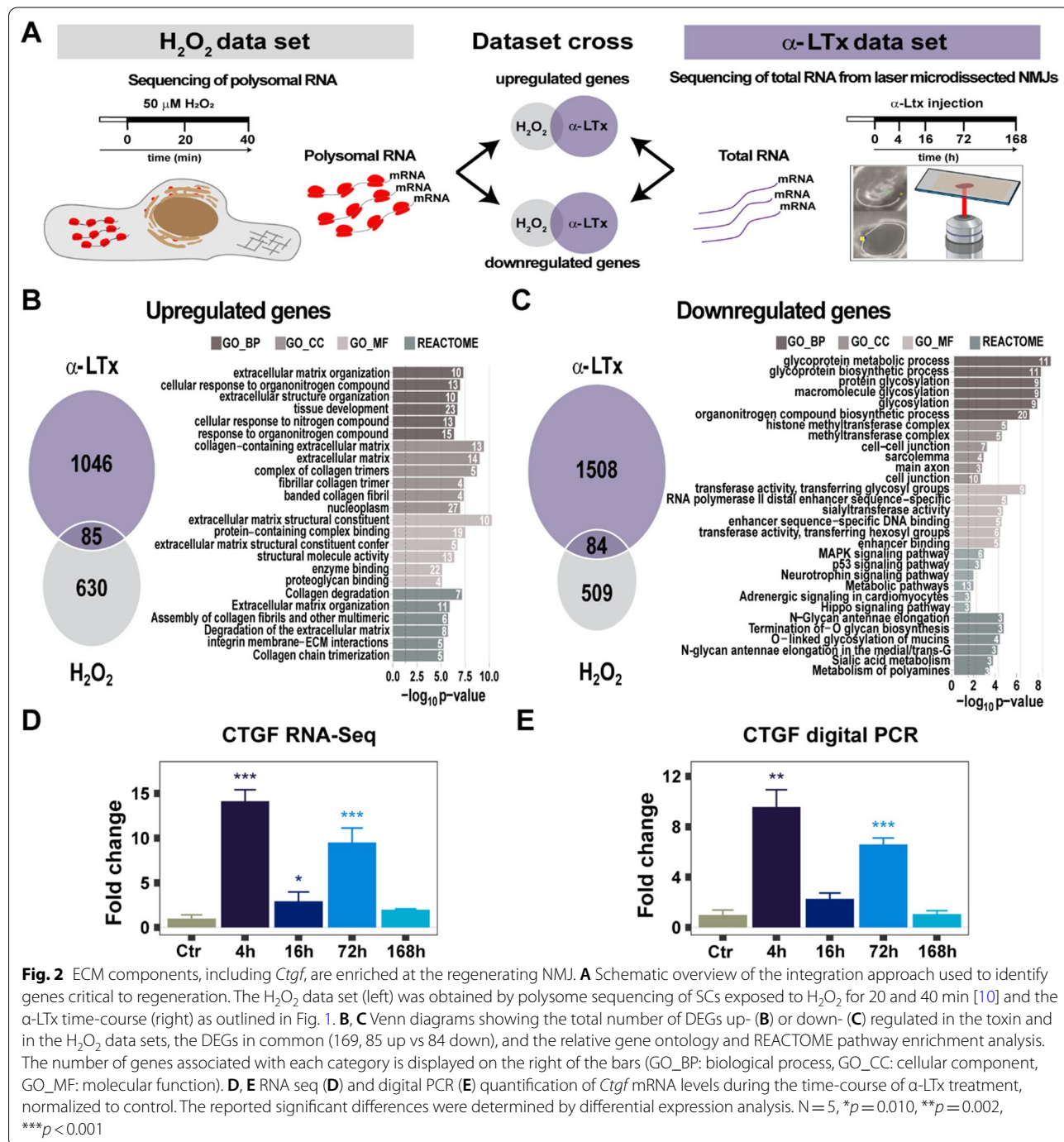
Hydrogen peroxide signaling at the regenerating NMJ

We previously reported that H₂O₂ is produced by mitochondria of stressed neurons and is a major SC activator

[20, 22, 23]. We therefore wanted to determine whether this important *alarm* molecule was driving some of the transcriptomic changes we observed at the regenerating NMJ.

We thus cross compared the α -LTx-induced NMJ DEGs with our previously published data set of actively translated RNAs associated with polysomes purified from H_2O_2 -treated primary SCs [23] (Fig. 2A). Common genes

were defined by the intersection of genes up- or down-regulated in at least one time point of both α -LTx and H_2O_2 treatments. A total of 169 common DEGs (85 up and 84 down, Additional file 4) were identified, and the relative Gene Ontology enrichments are herein reported (Fig. 2B, C and Additional file 5). The 85 common up-regulated genes are enriched in structural and signalling ECM components (Fig. 2B, and Additional file 6). Among



the top common up-regulated genes, we focused on the transcript encoding the matricellular protein Ctgf, whose involvement in peripheral nerve regeneration in mice had not been previously addressed. Noticeably, at the intoxicated NMJ, up-regulation of *Ctgf* mRNA follows a biphasic trend, with an early peak, during the acute phase of degeneration (4 h), and a second increase 72 h post-intoxication, during regeneration (Fig. 2D). This trend was confirmed by digital PCR (Fig. 2E). Remarkably, *Ctgf* up-regulation at the NMJ matches the previously reported trend of *Ctgf* mRNA during nerve regeneration in *bridge* SCs [46] (Additional file 1: Fig. S3C). Consistent with a possible role of Ctgf in regeneration at the neuromuscular synapse, most Ctgf receptors ($\alpha_1\beta_3$, $\alpha_6\beta_1$, $\alpha_5\beta_1$, p75NTR, LRP-1, LRP-6) are expressed in our soleus NMJ data set.

These results suggest that H_2O_2 triggers ECM remodeling at the regenerating NMJ, and that temporal waves of *Ctgf* up-regulation may contribute to this process.

Ctgf localizes to the murine NMJ and promotes its functional recovery upon injury

To assess the presence of Ctgf at the NMJ, we performed immunofluorescence analysis of the *levator auris longus* (LAL), a thin muscle suitable for whole mount imaging [47]. In non-injured NMJs, we determined that Ctgf localizes to PSCs and in the extracellular space (Additional file 1: Fig. S4A upper panels), as confirmed by orthogonal projections and 3D reconstructions (Additional file 1: Fig. S4B, C and Additional file 7: Movie 1).

MAT degeneration and regeneration induced by α -LTx results in the progressive loss and reappearance of NF (Additional file 1: Figs. S1, S4A). During this process, we identified that Ctgf is redistributed at the synapse, becoming more extracellular, as shown by immunofluorescence (Additional file 1: Fig. S4A lower panels), and 3D reconstructions of α -LTx-treated NMJs (Additional file 8: Movie 2).

The increase in *Ctgf* transcript (Fig. 2D, E) is likely to be initiated by *alarm* signals (including H_2O_2) released by degenerating motor axons that activate SCs [20, 22, 23, 48]. In support of this possibility, we found that α -LTx exposure increases Ctgf availability in SCs co-cultured with spinal cord motor neurons (SCMNs) (Additional file 1: Fig. S5A, B), and that H_2O_2 treatment similarly rapidly increases Ctgf levels and release (Additional file 1: Fig. S5C–E).

To assess the contribution of Ctgf to MAT regeneration, we intraperitoneally injected a Ctgf-neutralizing IgG monoclonal antibody before the local injection of α -LTx in the hind limb of mice. Neurotransmission was evaluated by recording the evoked junctional potentials (EJPs) of soleus muscle fibres 96 h later, when $\approx 50\%$ of

neurotransmission is rescued at intoxicated NMJs. We discovered that functional recovery of the NMJ is significantly delayed upon Ctgf neutralization (Fig. 3A). This result is corroborated by immunostaining of the pre-synaptic markers syntaxin and VAMP1, which showed that Ctgf neutralization also impaired anatomical rescue, with fewer NMJs displaying re-innervation (Fig. 3B, C). It is important to note that, as expected, there is only a partial impairment in regeneration upon Ctgf neutralization, as additional factors contribute to the process [1–4, 6, 7, 9, 10].

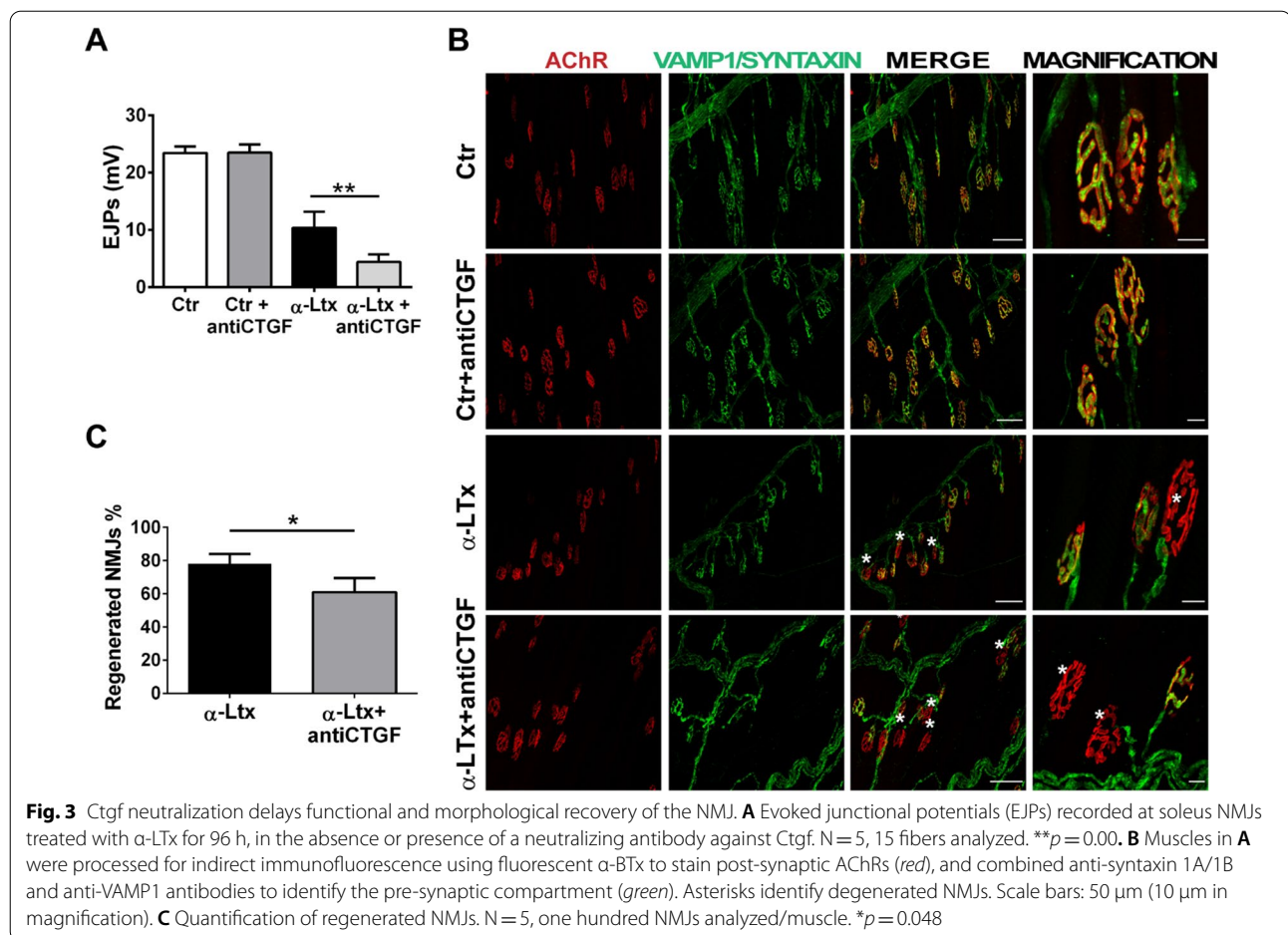
Local hydrogen peroxide production upon nerve injury drives Ctgf production

To extend our findings at the NMJ to additional models of nerve damage and evaluate the possibility that the local production of H_2O_2 by neurons is a general injury response, we assessed H_2O_2 levels in the sciatic nerve of live, anaesthetized mice before and after nerve compression by injecting the H_2O_2 -specific fluorescent probe PF6-AM [42] beneath the sciatic nerve epineurium. Strikingly, nerve crush induces H_2O_2 generation close to the injury site within two minutes of damage (Fig. 4A, B). At the end of each experiment, 1 mM H_2O_2 was applied as a positive control (A, bottom panel).

To shed light on the origin of H_2O_2 , we bathed the sciatic nerve prior to crush in either the NADPH oxidase (NOX) inhibitor VAS2870 or the mitochondria-targeted antioxidant MitoTEMPO. Inhibition of NOX activity had no impact on the injury-induced increase in H_2O_2 (Fig. 4C, D), while MitoTEMPO treatment restricted the production of this *alarm* signal (Fig. 4E, F), indicating that the upsurge in H_2O_2 signaling in the damaged sciatic nerve is derived from mitochondria, a finding in agreement with our previous observations at the intoxicated MAT [20].

Since toxin-induced nerve injury results in increased Ctgf availability at the regenerating NMJ (Fig. 2D, E and Additional file 1: Fig. S4A), we assessed whether a similar upregulation in Ctgf occurs upon sciatic nerve injury. Whole mount immunofluorescence analysis showed strong increases in Ctgf following either a compression or a transection of the sciatic nerve (Fig. 5A, longitudinal view). These findings were replicated in analyses of nerve cross-sections collected over the lesion site, both in response to compression (Fig. 5B, C) and to transection (Fig. 5D, E). Confirming successful lesions, we observed NF loss due to motor axon degeneration, and a global Ctgf increase in myelinating SCs, as well as in other cell types within the nerve (Fig. 5B–E).

To determine the role of H_2O_2 in the local upregulation of Ctgf in response to nerve lesion, we pre-treated nerves by injection with catalase, which restricts H_2O_2



availability by converting it to H₂O and O₂. Catalase treatment dampened the increase in Ctgf levels (Fig. 6A, longitudinal view, and 6B-C, cross sections and relative quantification), indicating that H₂O₂ is an important mediator of the Ctgf production.

Ctgf promotes neurotransmission recovery and polarized axonal elongation in the injured sciatic nerve

Ctgf plays a role in functional and anatomical recovery at the intoxicated NMJ (Fig. 3); we thus performed antibody neutralization experiments to determine whether the increased Ctgf availability upon sciatic nerve injury aids regeneration. To do so, we intraperitoneally injected anti-Ctgf neutralizing antibody once per week after nerve crush, and assessed functional recovery at 18 and 28 days. Reducing Ctgf availability delayed neurotransmission rescue of crushed sciatic nerves at both time points, as shown by electromyographic recordings of the compound muscle action potentials (CMAP) in gastrocnemius muscles (Fig. 7A). In contrast with untreated mice, CMAP traces from injured sciatic nerves treated with the Ctgf-neutralizing antibody maintain a disrupted,

polyphasic shape 28 days post-nerve damage, further supportive of delayed recovery (Fig. 7B).

We also assessed regeneration with and without Ctgf neutralisation after nerve transection. In line with findings post-crush, Ctgf neutralisation caused reduced and misdirected motor axon elongation after cut, as shown by NF and GAP-43 (growth-associated protein) distribution in whole mount nerve preparations (Fig. 7C), and by Tomato-expressing ChAT-positive axons that underwent the same experimental protocol (Fig. 7D).

Ctgf aids polarized axonal re-growth by guiding SC migration

Neurotransmission blockade by α -Ltx leads to a change in the shape of PSCs that extend processes or sprouts emerging from the paralyzed endplates. This response is particularly evident in slow-twitch muscles like the soleus (Additional file 1: Fig. S6A, upper panels), and assists and drives the sprouting of neurons [16, 49]. Sprouts represent a plastic, compensatory response of PSCs and motor axons to neurotransmission impairment, and mark the initiation of motor axon regeneration. Strikingly, we

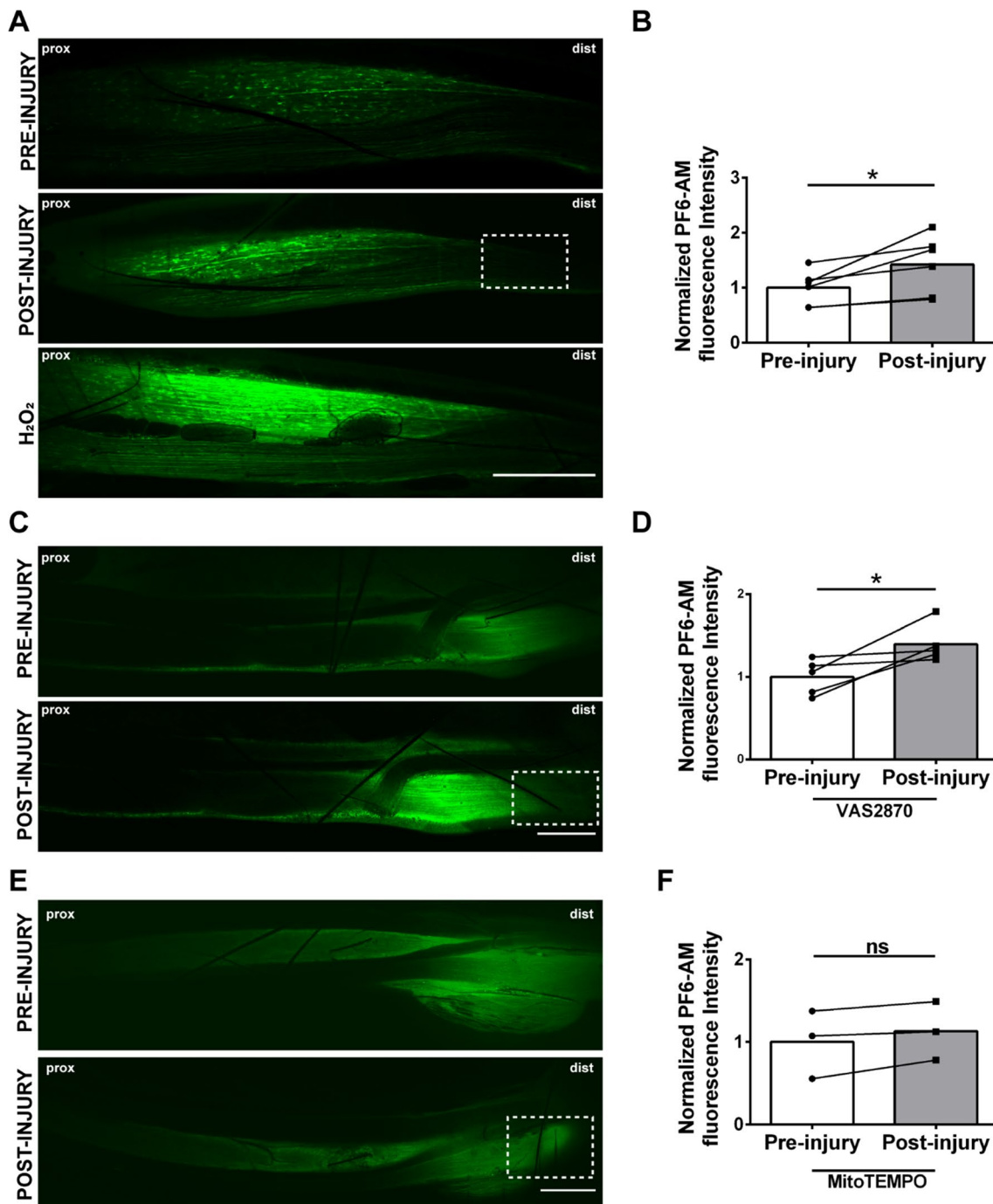


Fig. 4 H₂O₂ is rapidly produced upon compression of the sciatic nerve and originates from mitochondria. **A, B** Imaging of H₂O₂ production in the sciatic nerve of a live, anaesthetized mouse before (**A**, upper panel) and after (**A**, middle panel) sciatic nerve crush, and quantification of PF6-AM signal (**B**, **p* = 0.029). The dotted squares indicate the lesion site. Lower panel: PF6-AM fluorescence in response to 1 mM H₂O₂ (positive control). Scale bar: 500 μm. **C, D** H₂O₂ increase following sciatic nerve crush is unaffected by the NOX inhibitor VAS2870. Scale bar: 500 μm. Quantification of PF6-AM signal is shown in **D**. N = 3, **p* = 0.045. **E, F** H₂O₂ increase upon sciatic nerve crush is abolished by MitoTEMPO incubation. Scale bar: 500 μm. Quantification of PF6-AM signal is shown in **F**. N = 3, *p* = 0.123, ns = not significant

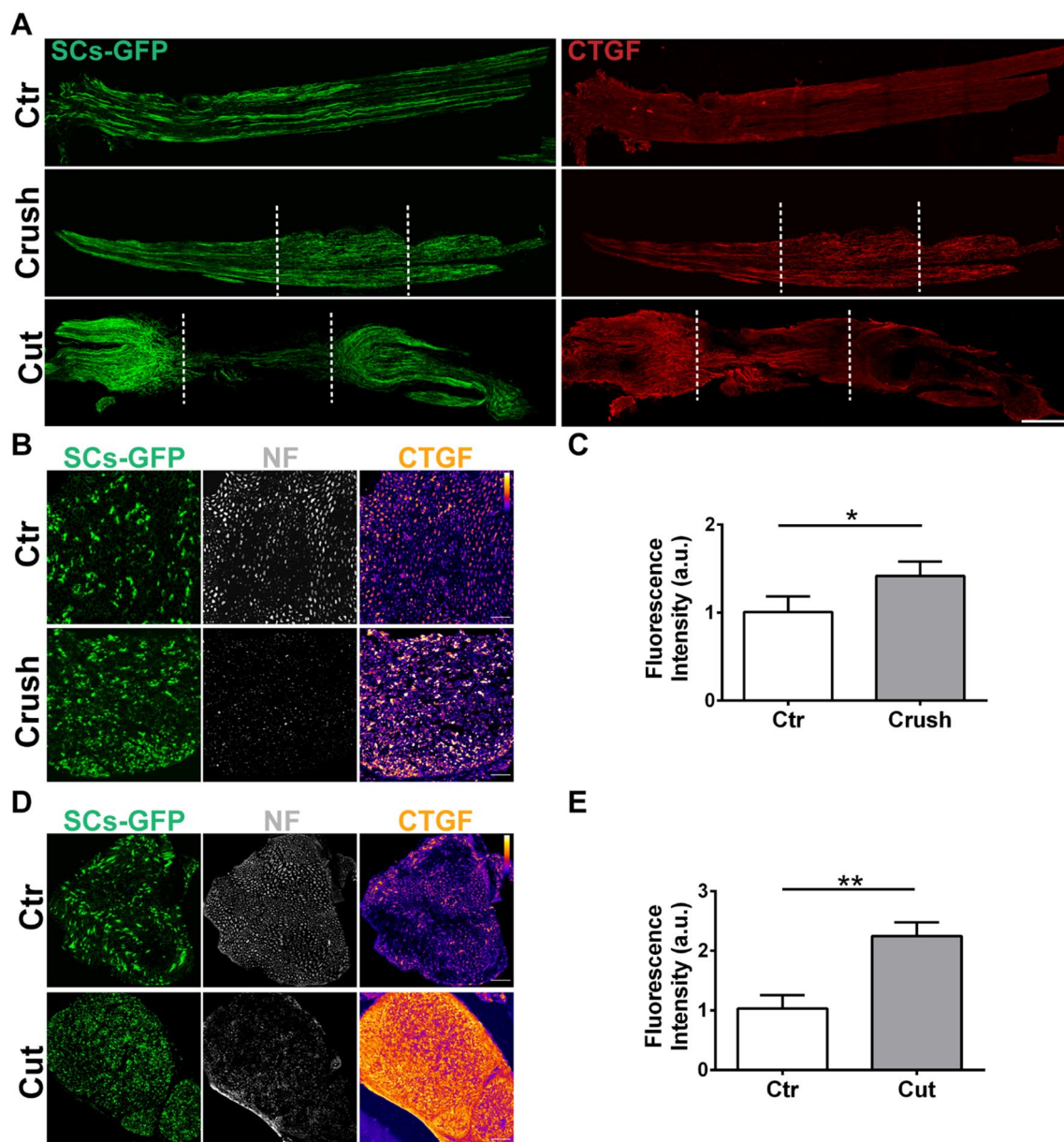
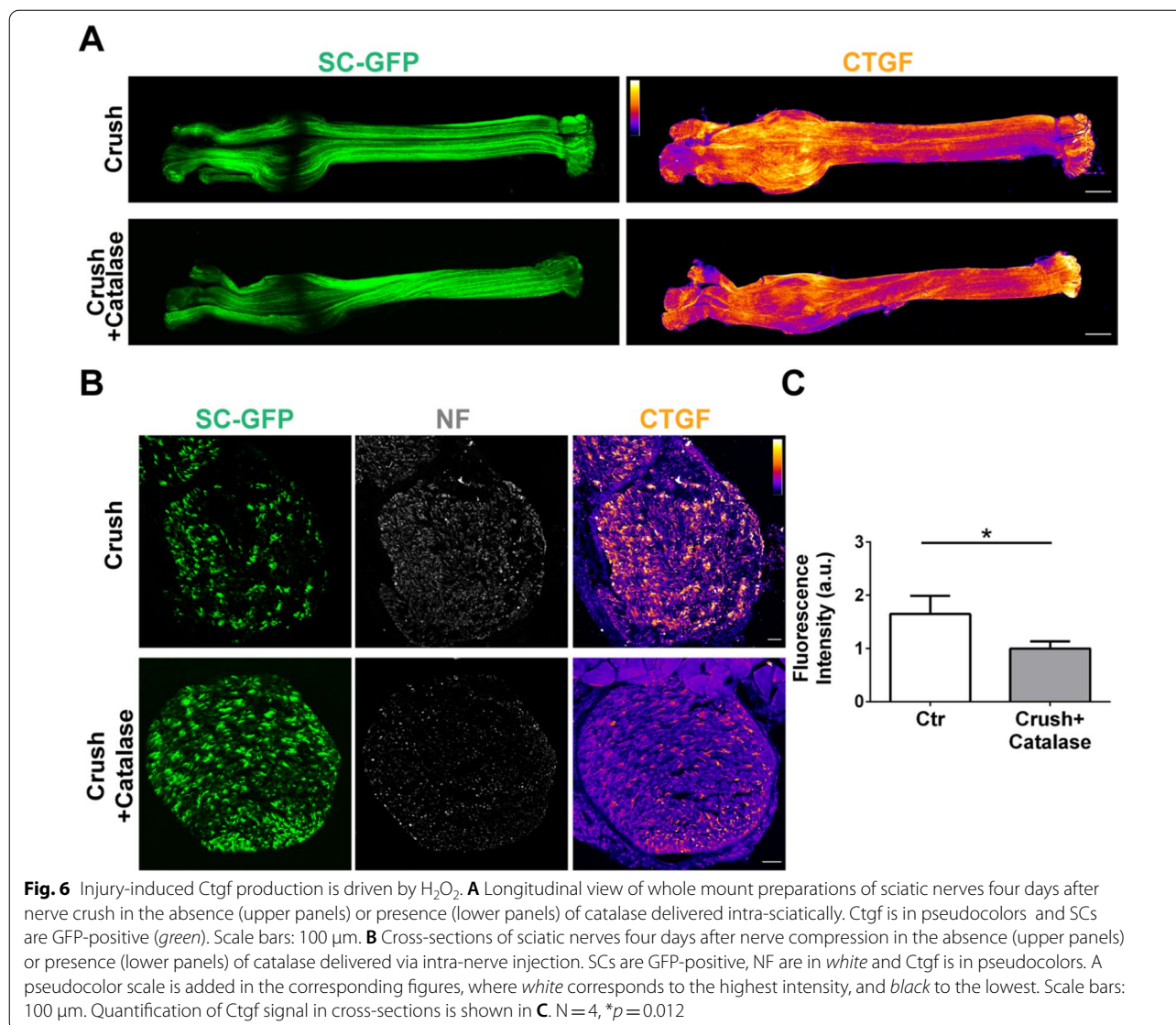


Fig. 5 Sciatic nerve injury drives increased Ctgf levels. **A** Longitudinal views of whole mount preparations of sciatic nerves from control mice (Ctr, upper panels), four days after nerve compression (crush, middle panels), and six days after nerve transection (cut, lower panels). Dotted lines indicate the injury site. Ctgf is in red and SCs are GFP-positive (green). Scale bar: 100 μ m. **B, D** Cross-sections of sciatic nerves in control conditions (Ctr, upper panels), four days after nerve compression (**B**), and six days after nerve transection (**D**). SCs are GFP-positive (green), NF in white, Ctgf is in pseudocolors. A pseudocolor scale is added in the corresponding figures, where white corresponds to the highest intensity, and black to the lowest. Scale bars: 50 μ m. **C, E** Quantification of Ctgf signal in cross sections. N=3, * p =0.041 (**C**), ** p =0.003 (**E**)

observed that PSC sprouts are Ctgf-positive (Additional file 1: Fig. S6A, upper panels, and Additional file 8: Movie 2). 3D reconstructions in Additional file 1: Fig. S6B allows a better visualization of Ctgf-positive sprouts in PSCs. These observations suggest that this protein may exert a pro-regenerative activity by sustaining/guiding axonal growth.

To test this hypothesis, we paralyzed the NMJ either by denervation (Additional file 1: Fig. S6A, middle panels), or by treatment with botulinum neurotoxin A (BoNT/A) (Additional file 1: Fig. S6A, lower panels), and monitored the presence of Ctgf in sprouts. In all the three conditions tested (reversible degeneration by α -LTx, sciatic nerve transection, and functional



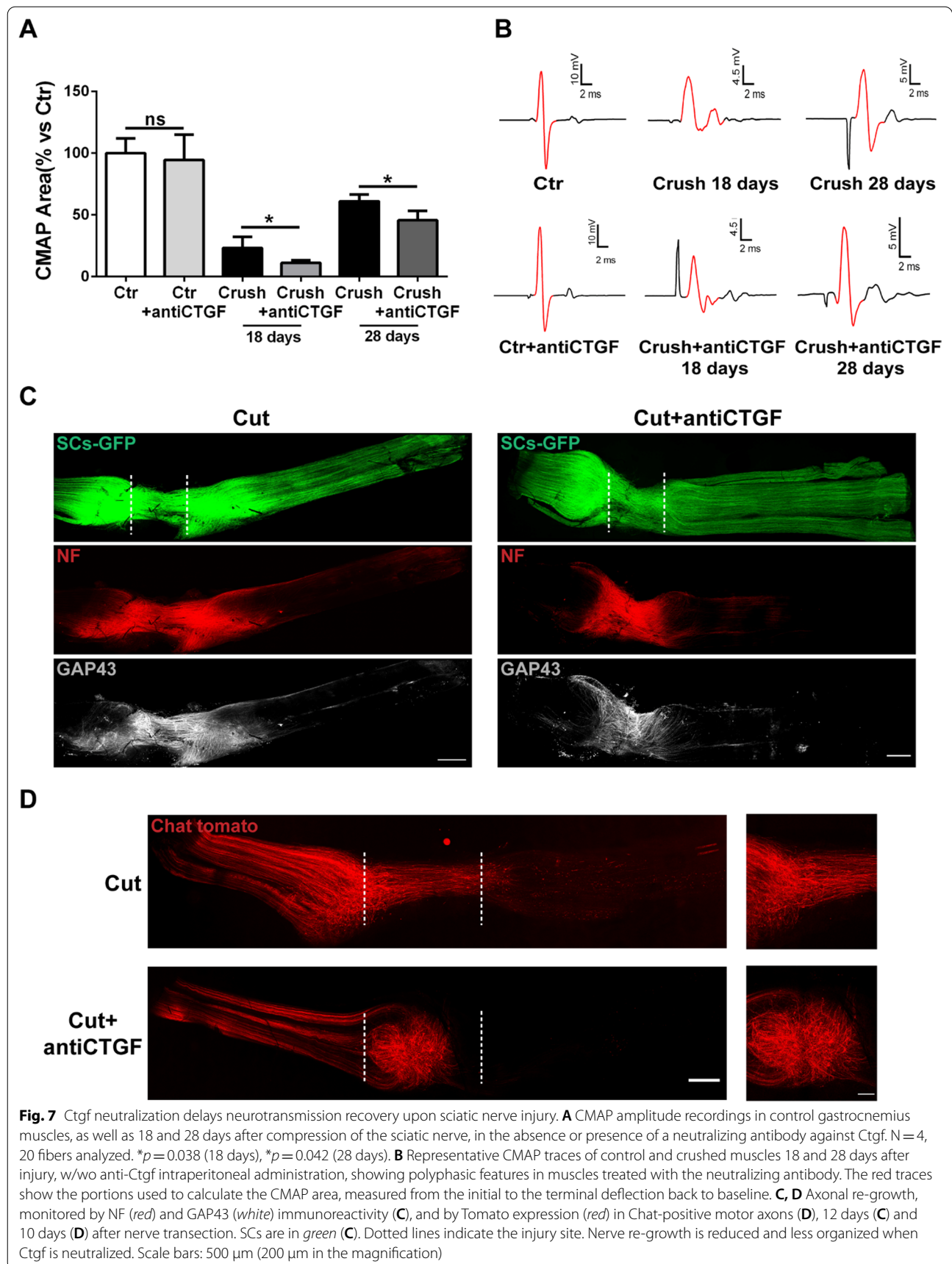
denervation by BoNT/A), PSC processes express Ctgf, suggesting that the molecule may indeed support PSC sprouting and, in turn, axonal elongation. Accordingly, Ctgf neutralization reduces the sprouts emerging from the MAT paralyzed by BoNT/A (Additional file 1: Fig. S6C, D). Mirroring this and providing further evidence of the ability of Ctgf to support SC migration, we observed faster wound healing upon scratching by SCs plated on a coating of recombinant Ctgf plus laminin, compared to SCs grown on laminin alone (Additional file 1: Fig. S6E, F). To extend these findings in vivo, we performed nerve transection experiments and showed that Ctgf neutralisation delays SC migration along the bridge, which is the new tissue that forms after cutting to reconnect the two axonal stumps (Fig. 8A).

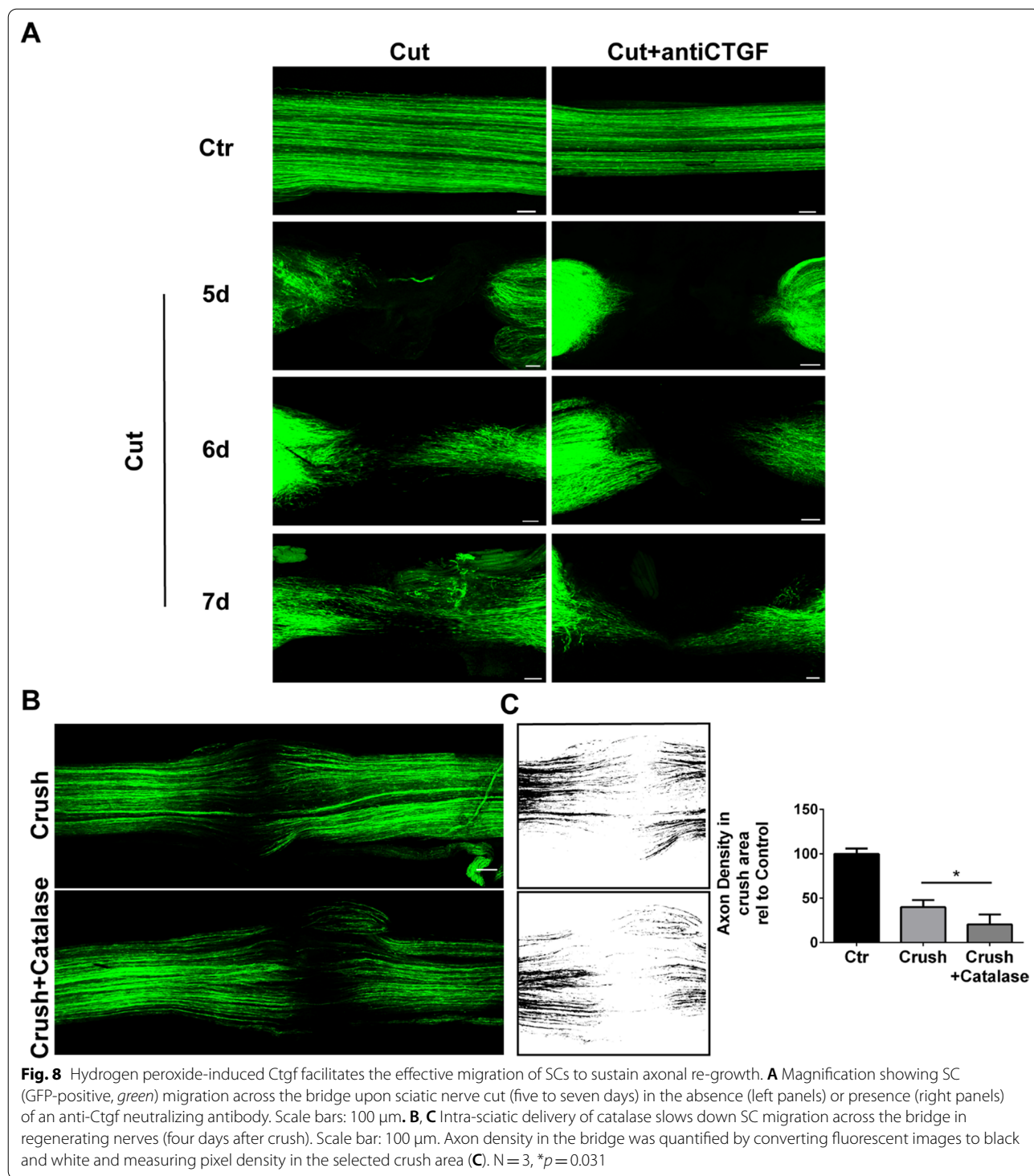
Moreover, and in line with the H₂O₂-dependent expression of Ctgf, H₂O₂ neutralization by treatment with catalase slows down SC migration across the bridge in regenerating nerves (Fig. 8B, C).

Overall, these findings support the hypothesis that H₂O₂ and its downstream product Ctgf are pro-regenerative factors that guide axonal growth along the trajectories provided by Ctgf-expressing SCs.

H₂O₂ signals through the YAP pathway to drive Ctgf transcription

Several signaling pathways converge on Ctgf transcription, including the transcription factors TEADs (Hippo signaling effectors) with their co-activators and Hippo transducers YAP/TAZ [50]. Given the emerging





importance of mechanosignaling for SC biology during development and in nerve regeneration, and in light of the fact that TEAD4 is upregulated in the NMJ transcriptome (Additional file 1: Fig. S3D), we looked at YAP expression and localization in response to H₂O₂

both in vivo and in vitro (Fig. 9). In the adult sciatic nerve, YAP expression in SCs is innervation-dependent (Fig. 9A upper panels and panel B); indeed, YAP disappears from denervated SCs, but reappears in SC nuclei during axonal regeneration [51]. To determine whether

H₂O₂ generated at the lesion site impacts the YAP signal in SC nuclei, we performed pre-crush intra-sciatic nerve injections of catalase and assessed YAP localization three and four days post-injury. YAP is still present in SCs nuclei three days after crush, when neurons start degenerating, and disappears the day after. Catalase treatment caused YAP to disappear from SCs already on day three after damage (Fig. 9A), suggesting that H₂O₂ sustains YAP transcriptional activity, which in turn drives *Ctgf* expression. Finally, we cultured SCs and exposed them to H₂O₂ in the presence of VT107, a pan-TEAD autopalmitylation inhibitor. VT107 treatment dampened the H₂O₂-mediated increase in *Ctgf* levels (Fig. 9C, D), suggesting that TEAD transcription factors are required to fully activate *Ctgf* expression.

Together, these findings indicate that production of the pro-regenerative factor *Ctgf* in SCs is both H₂O₂- and YAP-dependent.

Discussion

Peripheral nerves are able to regenerate in response to injury; however, the molecular events underlying this process remain to be fully resolved. To further our understanding into this crucial mechanism, we employed a range of in vitro and in vivo approaches that identified key roles for H₂O₂ and *Ctgf* in nerve regeneration. We found that in response to axon injury, mitochondria rapidly generate H₂O₂ to activate surrounding SCs. The local synthesis and release of H₂O₂ induce extensive transcriptional changes at the injured NMJ, particularly in genes encoding for ECM components, including the YAP-dependent *Ctgf* up-regulation. *Ctgf* contributes to functional recovery upon proximal and distal nerve damage by assisting SC migration and, in turn, allowing the oriented re-growth of the axons. The major findings of the present study are summarized in Fig. 10.

Regeneration of the NMJ is orchestrated by several signaling pathways that control synaptic plasticity and remodeling upon injury [1, 6, 10]. To dissect the molecular determinants driving NMJ regeneration, we took advantage of a highly specific pre-synaptic neurotoxin as a model of acute and reversible degeneration of the nerve terminal, and profiled the transcriptional changes taking place at the murine NMJ during intoxication, revealing a striking ECM remodeling triggered by nerve injury. To address whether this process is triggered by H₂O₂, a

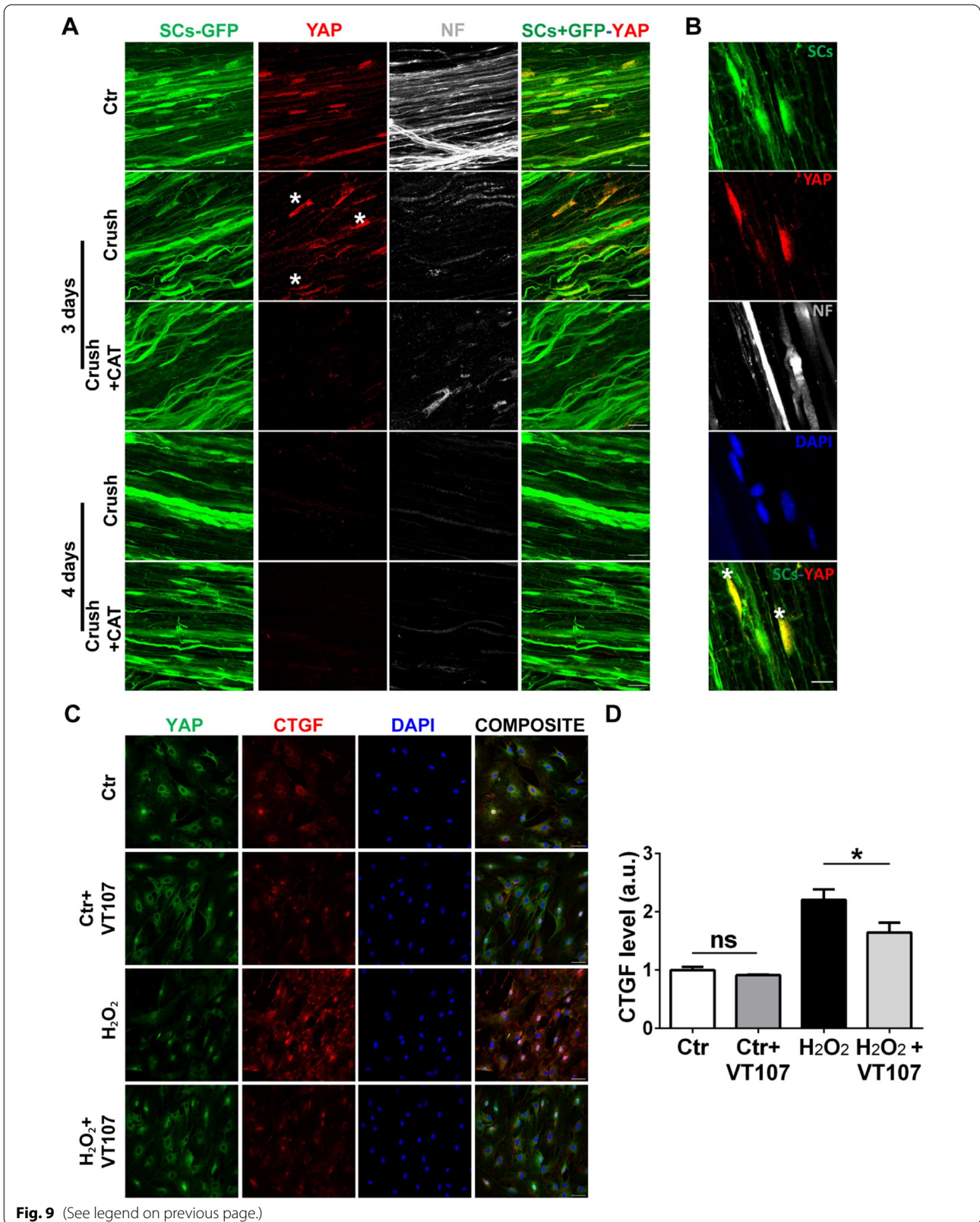
major SC activator and a pro-regenerative factor [20, 22, 23], we cross-referenced the transcriptomic changes identified at α -LTx poisoned NMJs with those previously obtained from H₂O₂-treated primary SCs [23], identifying 169 common DEGs. Several of the 85 common up-regulated transcripts encode for ECM components (both structural and signaling members), among them the matricellular protein *Ctgf*. Matricellular proteins do not participate in ECM structural integrity, but rather act as modulators in a variety of cellular responses [25]. They are highly expressed during development or upon injury and, once secreted and sequestered in the extracellular space, they bind to the structural matrix and transduce signalling cascades, or contribute to activation of cytokines, growth factors, and proteases in the pericellular space. They also display de-adhesive activities, which likely contribute to tissue remodelling following injury, or in disease states. Indeed, matricellular proteins are involved in highly dynamic processes like wound healing, cancer, and in the production of connective tissue [52]. As the *Ctgf* transcript is part of the 'H₂O₂ signature', is increased during MAT degeneration and recovery, encodes for a matricellular protein involved in tissue remodelling, and is required for zebrafish spinal cord regeneration [53], we investigated for the first time in mice the cellular origin and the molecular determinants of *Ctgf* production, and its role in peripheral nerve regeneration.

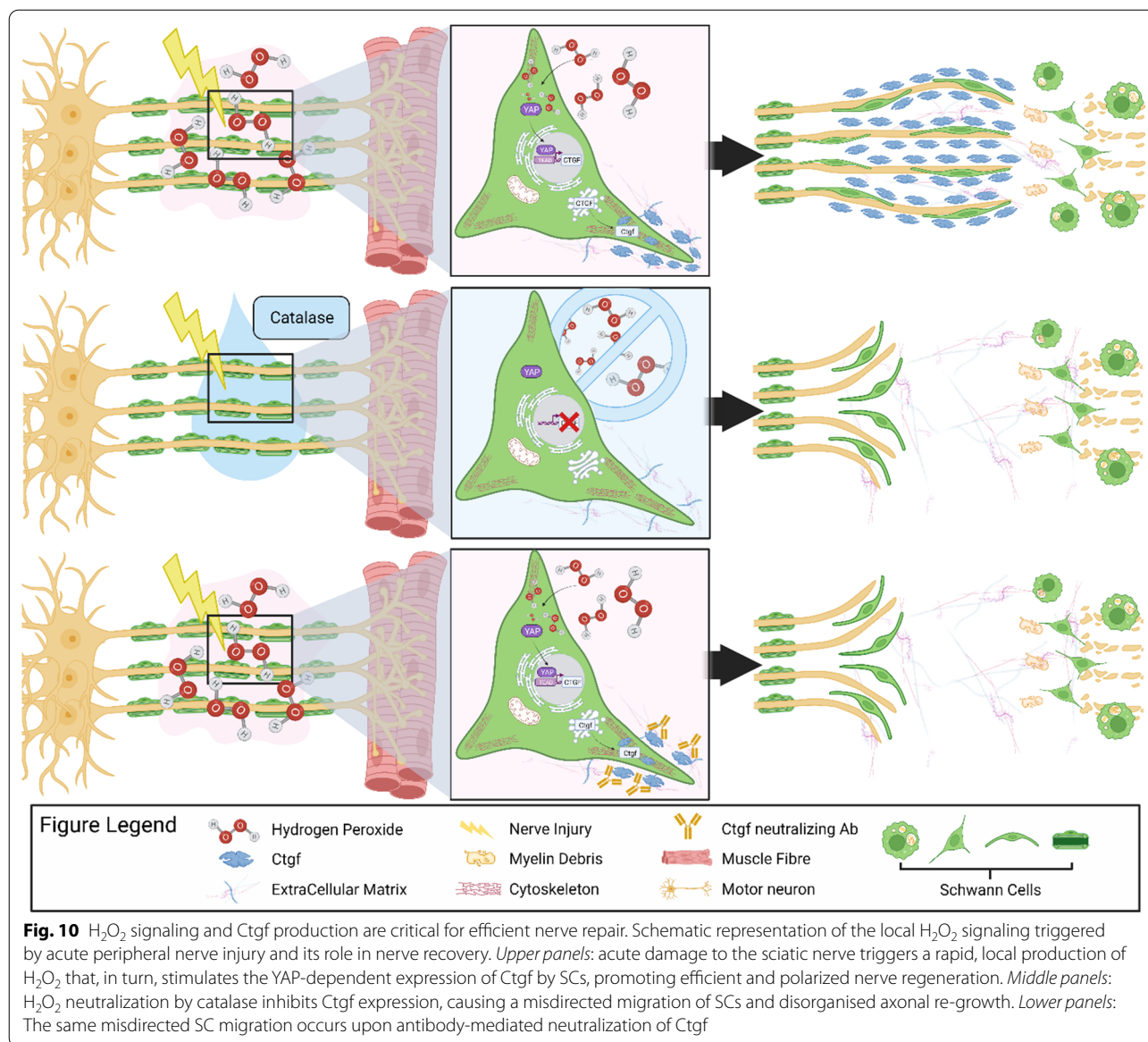
At the intoxicated NMJ, the expression of *Ctgf* mRNA strongly increases during the acute phase of degeneration, with a second peak during regeneration. *Ctgf* localizes in PSCs and in the extracellular space, and promotes the functional recovery of the NMJ, as *Ctgf* neutralization by a specific antibody delays MAT regeneration following the acute injury by α -LTx. Arguably, *Ctgf* expression is triggered by *alarmins* from degenerating MAT: indeed H₂O₂, a major neuronal *alarm* signal, and a strong mediator of NMJ rescue, promotes *Ctgf* synthesis and release by primary SCs. Overall, injury signals released by damaged MNs induce *Ctgf* expression by SCs.

A novel and important finding reported here is that H₂O₂ is rapidly generated in the sciatic nerve upon damages that mimic traumatic injuries in humans (e.g., compression or transection), and this inter-cellular signaling drives *Ctgf* expression. Pro-regenerative axonal reactive oxygen species (ROS) signaling was recently found to

(See figure on next page.)

Fig. 9 *Ctgf* production upon nerve injury is H₂O₂- and YAP-dependent. **A** YAP (red) expression and localization in SCs (expressing GFP under the *plp*-promoter, green) in control nerves and 3/4 days post-crush, in the absence or presence of catalase delivered into the sciatic nerve. NF is in white and nuclei are stained with DAPI (blue). Asterisks mark YAP-positive SCs. Scale bars: 20 μ m. A magnification of YAP localization in control nerves is shown in panel **B**. Scale bar: 10 μ m. **C, D** Representative immunostaining of YAP and *Ctgf* in primary SCs exposed to 50 μ M H₂O₂ w/wo the pan-TEAD autopalmitylation inhibitor VT107 (**C**). YAP is in green, *Ctgf* in red and nuclei are in blue. Scale bars: 50 μ m. Quantification of *Ctgf* levels by ELISA is shown in **D**. N = 3, **p* = 0.0166, ns = not significant





occur in sensory neurons within a few hours from sciatic nerve crush, secondary to inflammatory signals coming from the inflammatory milieu [54]. It should be considered that the term ROS includes unstable and short-living species, such as the superoxide anion, which are unlikely to mediate any direct signaling given their rapid quenching. By converting superoxide anions into H₂O₂, the superoxide dismutase produces a more stable ROS species that can perform transfer from one cell to another, which is an absolute requirement for an inter-cellular mediator. Here, we not only identified H₂O₂ as the ROS species produced upon injury in the sciatic nerve of live, anaesthetized mice, but also found that it is generated by the mitochondria of injured nerves. Strikingly, this

localized H₂O₂ signal is detectable within a couple of minutes from nerve injury.

H₂O₂ triggers Ctgf generation close to the injury site mainly in SCs, and particularly in the *bridge*, a new tissue that forms upon nerve transection to reconnect the two stumps. Of note, *bridge* SCs are a peculiar sub-population of de-differentiated SCs that display pronounced mesenchymal features (in response to the microenvironment) and migratory behavior during nerve repair [46].

Ctgf consists of four functional domains that mediate its participation in several physiological actions. The N- and C-domains of Ctgf mediate distinct biological processes, *i.e.*, differentiation (collagen synthesis), and proliferation, respectively, in concert with other growth

factors [55]. Pro-fibrogenic properties of *Ctgf* are commonly ascribed to the N-terminus, and have been widely described in different pathological contexts. A human monoclonal antibody (FG-3019) raised against the N-domain of the molecule, is currently under evaluation in clinical studies for the treatment of idiopathic pulmonary fibrosis, pancreatic cancer, and Duchenne muscular dystrophy (DMD). In gastrocnemius muscles of *SOD1^{G93A}* mice at symptomatic stages (16 weeks), which show increased levels of *Ctgf*, administration of FG-3019 reduced fibrosis and ameliorated NMJ innervation [56]. *Ctgf* is up-regulated in skeletal muscles of *mdx* mice modelling DMD, and its genetic reduction in this model through crossing with heterozygous *CTGF[±]* mice leads to improved skeletal muscle isometric force, and decreased muscle fibrosis and damage [57]. In addition, in mice heterozygous for *Ctgf*, or upon FG-3019 treatment, there is an accumulation of ECM proteins after denervation, as compared to control mice, suggesting a direct role of *Ctgf* in denervation-induced fibrosis [58].

Conversely, very little is known about the pro-regenerative potential of *Ctgf*. One study in zebrafish [53] reports that *Ctgifa* supports glia proliferation and bridging, in turn promoting spinal cord regeneration. Our data support this notion of the pro-regenerative properties of *Ctgf*: these are likely ascribable to the C-terminus of the molecule, which is specifically targeted by the anti-*Ctgf* antibodies employed in our neutralization experiments.

Growing evidence supports a crucial role of the cellular milieu for the regeneration response [46], which likely influences *Ctgf* action; in fact, *Ctgf* may stimulate either cell proliferation or cell differentiation, depending on the presence or absence of additional growth factors and cytokines in the milieu. Accordingly, in tissue formation and in regeneration both processes occur, with cell proliferation preceding and then closely followed by differentiation [55]. Both zebrafish [53] and our mouse injury experimental models are competent for regeneration, at variance from that employed by Rebolledo and colleagues, where a small section of the nerve was removed after unilateral denervation to prevent re-innervation, making regeneration unfeasible [58]. Thus, the pro-regenerative context of the two models seems to be crucial to determine the exact role of *Ctgf* in regeneration.

Ctgf sustains nerve regeneration most likely via an axon growth promoting action. Indeed, in the absence of *Ctgf*, axonal re-growth is slower and appears less polarized, likely due to a slower and misdirected migration of SCs within the bridge, eventually leading to a delay in neurotransmission rescue. Of note, the *Ctgf* transcript increases in neurons responsible for collateral sprouting, which is a process where undamaged neurons react to an injury-induced environment

(Wallerian degeneration) by expanding sprouts that functionally synapse with denervated targets [59]. Along the same line, *Ctgf*-positive sprouts, which form in PSCs upon neurotransmission blockade (by either denervation, or intoxication), further support the view that SC-expressed *Ctgf* may play a role in supporting/guiding axonal elongation.

Ctgf expression may also rely on mechanical constraints, e.g., changes in the stiffness of ECM and/or loss of axonal contact caused by nerve damage. Indeed, context-dependent signalling can be sensed by SCs through mechanosensors and mechanotransducers [60–62] and, in turn, affect *Ctgf* gene expression. Accumulating evidence has described pivotal functions of the Hippo pathway in regulation of cell plasticity during mammalian development and tissue regeneration [63]: here we show that the transcriptional coactivator YAP, a major downstream effector of the Hippo pathway, drives *Ctgf* transcription in response to a local inter-cellular H_2O_2 signalling, paving the way for a future further investigation on the role of YAP-mediated mechanotransduction in peripheral nerve repair and in SC biology, and on the contribution of local H_2O_2 in such communication.

The present findings support the view that an intense inter-cellular signalling, of which H_2O_2 is a major player, occurs not only during development [7, 9], but also in adulthood, and drives peripheral nerve regeneration. Moreover, it highlights how our time-series transcriptional profiling of the regenerating NMJ represents a powerful source of novel candidate molecules that can be harnessed to support regeneration in different peripheral nerve injuries and possibly neuropathies.

Abbreviations

BoNT/A: Botulinum neurotoxin type A; ChAT: Choline acetyltransferase; *Ctgf*: Connective tissue growth factor; DEG: Differentially expressed genes; GAP-43: Growth-associated protein 43; H_2O_2 : Hydrogen peroxide; α -Ltx: α -Latrotoxin; MAT: Motor axon terminal; MN: Motor neuron; NF: Neurofilament; NMJ: Neuromuscular junction; NOX: NADPH oxidase; PSC: Perisynaptic Schwann cell; ROS: Reactive oxygen species; SC: Schwann cell; SCMN: Spinal cord motor neuron; SNAP-25: Synaptosomal-associated protein, 25 kDa; TEAD: TEA domain family member 4; VAMP: Vesicle associated membrane protein; YAP: Yes-associated protein.

Supplementary Information

The online version contains supplementary material available at <https://doi.org/10.1186/s40478-022-01495-5>.

Additional file 1. Supplementary figures.

Additional file 2: Table S1. Differential analyses of gene expression at the α -Ltx-poisoned soleus NMJs during degeneration and regeneration. Differential analyses comparing gene expression at the α -Ltx-poisoned soleus NMJs at the four time points analyzed with respect to controls. Log₂-fold change, p-value and class (- down-regulated, + up-regulated, = invariant), and the average count of reads per million (CPM) are reported for each gene and each time point.

Additional file 3: Table S2. Gene ontology and REACTOME analysis of α -LTx data set. Gene ontology and REACTOME pathways enrichment analysis of DEGs of the α -LTx data set (down- and up-regulated) at each time point. The number and the list of DEGs associated to significant terms are reported.

Additional file 4: Table S3. Intersection of α -LTx and H2O2 data sets.

Additional file 5: Table S4. Gene ontology and REACTOME analysis of α -LTx-H2O2 common DEGs Intersection of DEGs of the α -LTx data set with those induced by H2O2, previously identified in [23]. The class (- down-regulated, + up-regulated, = invariant) of each gene of the two data sets is reported.

Additional file 6: Table S5. List of up-regulated ECM terms shared by the α -LTx and the H2O2 data sets. Selection of GO and REACTOME terms associated to the ECM emerging from the intersection of up-regulated genes of the α -LTx and the H2O2 data sets.

Additional file 7: Movie 1. 3D movie showing Ctgf localization in a control soleus NMJ.

Additional file 8: Movie 2 3D movie showing Ctgf localization in a degenerated soleus NMJ.

Additional file 9: Table 6. List of antibodies employed in the study and relative information.

Acknowledgements

We are grateful to Michele Menicagli and Paolo Aretini (Pisa Science Foundation) for help with laser microdissection and bioinformatics, respectively. We gratefully acknowledge the support and suggestions of Prof. Cesare Montecucco (CM).

Author contributions

SN and MR conceived and designed the study. SN, MS, GD, MP and AM performed the imaging and the electrophysiological experiments, and analysed the results. SN, APT and JNS performed live imaging experiment under the supervision of GS. FL, TT, GV, GS, CR, SF and FL performed the bioinformatical analysis, with major contribution by FL. FL and CMM performed the RNA sequencing. The first draft of the manuscript was written by MR and all authors commented on previous versions of the manuscript. All authors read and approved the final manuscript.

Funding

This research was funded by Ministero della Difesa, Progetto RIPANE (MONT_COMM18_03) to CM and FL, by Provincia Autonoma di Trento (Bando Grandi Progetti 2012, AXonomIX, "Identifying the translational networks altered in motor neuron diseases") to CM and GV, by the Interomics project of the CNR to CM, by a Junior Non-Clinical Fellowship from the Motor Neuron Disease Association (Tosolini/Oct20/973–799) to APT, by the Medical Research Council Career Development Award (MR/S006990/1) to JNS, by Wellcome Senior Investigator Awards (107116/Z/15/Z and 223022/Z/21/Z) to GS, by a UK Dementia Research Institute Foundation award (UKDRI-1005) to GS, by an EMBO short-term fellowship to SN, and by the University of Padua to MR. MS and GD'E were recipients of PhD fellowships by the Cariparo Foundation and the University of Padua, respectively. GV acknowledges funding from AriSLA Foundation (AxRibALS), FaL from CARITRO.

Availability of data and materials

Raw and analyzed RNA-seq data generated in this study have been deposited in the Gene Expression Omnibus (GEO) under the accession code GSE154547. Part of the data are included as electronic supplementary material.

Declarations

Ethics approval and consent to participate

All information is provided in the Methods section.

Competing interests

The authors have no financial or non-financial interests to disclose.

Author details

¹Department of Biomedical Sciences, University of Padua, 35131 Padua, Italy. ²U.O.C. Clinica Neurologica, Azienda Ospedale, University of Padua, 35128 Padua, Italy. ³Institute of Biophysics, CNR Unit at Trento, 38123 Povo, Italy. ⁴Department of Cellular, Computational and Integrative Biology (CIBIO), University of Trento, 38123 Povo, Italy. ⁵Section of Hematology, Department of Internal Medicine, Yale Comprehensive Cancer Center, Yale University School of Medicine, New Haven, CT 06520, USA. ⁶Myology Center (CIR-Myo), University of Padua, 35129 Padua, Italy. ⁷Padua Neuroscience Center, University of Padua, 35131 Padua, Italy. ⁸Laboratory of Genomics, Pisa Science Foundation, 56017 San Giuliano Terme, Italy. ⁹Department of Biology, University of Padua, 35131 Padua, Italy. ¹⁰Center of Medical and Veterinary Research of the Ministry of Defence, 00184 Rome, Italy. ¹¹Department of Neuromuscular Diseases, Queen Square Institute of Neurology, University College London, London WC1N 3BG, UK. ¹²UCL Queen Square Motor Neuron Disease Centre, University College London, London WC1N 3BG, UK. ¹³UK Dementia Research Institute, University College London, London WC1E 6BT, UK.

Received: 26 August 2022 Accepted: 12 December 2022

Published online: 25 December 2022

References

- Brosius Lutz A, Barres BA (2014) "Contrasting the glial response to axon injury in the central and peripheral nervous systems," (in eng). *Dev Cell* 28(1):7–17. <https://doi.org/10.1016/j.devcel.2013.12.002>
- Gordon T (2016) "Nerve regeneration in the peripheral and central nervous systems," (in eng). *J Physiol* 594(13):3517–3520. <https://doi.org/10.1113/JP270898>
- Fawcett JW, Keynes RJ (1990) "Peripheral nerve regeneration," (in eng). *Annu Rev Neurosci* 13:43–60. <https://doi.org/10.1146/annurev.ne.13.030190.000355>
- Jessen KR, Mirsky R (2016) "The repair Schwann cell and its function in regenerating nerves," (in eng). *J Physiol* 594(13):3521–3531. <https://doi.org/10.1113/JP270874>
- Tedeschi A (2011) "Tuning the orchestra: transcriptional pathways controlling axon regeneration," (in eng). *Front Mol Neurosci* 4:60. <https://doi.org/10.3389/fnmol.2011.00060>
- Zelada D, Bermedo-García F, Collao N, Henríquez JP (2021) "Motor function recovery: deciphering a regenerative niche at the neuromuscular synapse," (in eng). *Biol Rev Camb Philos Soc* 96(2):752–766. <https://doi.org/10.1111/brv.12675>
- Darabid H, Perez-Gonzalez AP, Robitaille R (2014) "Neuromuscular synaptogenesis: coordinating partners with multiple functions," (in eng). *Nat Rev Neurosci* 15(11):703–718
- Sanes JR, Lichtman JW (2001) "Induction, assembly, maturation and maintenance of a postsynaptic apparatus," (in eng). *Nat Rev Neurosci* 2(11):791–805. <https://doi.org/10.1038/35097557>
- Sanes JR, Lichtman JW (1999) "Development of the vertebrate neuromuscular junction," (in eng). *Annu Rev Neurosci* 22:389–442. <https://doi.org/10.1146/annurev.neuro.22.1.389>
- Rigoni M, Negro S (2020) "Signals orchestrating peripheral nerve repair," (in eng). *Cells* 9(8):07. <https://doi.org/10.3390/cells9081768>
- Vinsant S et al (2013) "Characterization of early pathogenesis in the SOD1(G93A) mouse model of ALS: part II, results and discussion," (in eng). *Brain Behav* 3(4):431–457. <https://doi.org/10.1002/brb3.142>
- Alhindi A, Boehm I, Chaytow H (2021) "Small junction, big problems: Neuromuscular junction pathology in mouse models of amyotrophic lateral sclerosis (ALS)," (in eng). *J Anat*. <https://doi.org/10.1111/joa.13463>
- Rocha MC, Pousinha PA, Correia AM, Sebastião AM, Ribeiro JA (2013) "Early changes of neuromuscular transmission in the SOD1(G93A) mice model of ALS start long before motor symptoms onset," (in eng). *PLoS ONE* 8(9):e73846. <https://doi.org/10.1371/journal.pone.0073846>
- Clark JA, Southam KA, Blizzard CA, King AE, Dickson TC (2016) "Axonal degeneration, distal collateral branching and neuromuscular junction architecture alterations occur prior to symptom onset in the SOD1(G93A) mouse model of amyotrophic lateral sclerosis," (in eng). *J Chem Neuroanat* 76:35–47. <https://doi.org/10.1016/j.jchemneu.2016.03.003>

15. Pun S, Santos AF, Saxena S, Xu L, Caroni P (2006) "Selective vulnerability and pruning of phasic motoneuron axons in motoneuron disease alleviated by CNTF," (in eng). *Nat Neurosci* 9(3):408–419. <https://doi.org/10.1038/nn1653>
16. Frey D, Schneider C, Xu L, Borg J, Spooren W, Caroni P (2000) "Early and selective loss of neuromuscular synapse subtypes with low sprouting competence in motoneuron diseases," (in eng). *J Neurosci* 20(7):2534–2542
17. Wishart TM, Parson SH, Gillingwater TH (2006) "Synaptic vulnerability in neurodegenerative disease," (in eng). *J Neuropathol Exp Neurol* 65(8):733–739. <https://doi.org/10.1097/01.jnen.0000228202.35163.c4>
18. Duchen LW, Gomez S, Queiroz LS (1981) "The neuromuscular junction of the mouse after black widow spider venom," (in eng). *J Physiol* 316:279–291
19. Ushkaryov YA, Rohou A, Sugita S (2008) "alpha-Latrotoxin and its receptors," (in eng). *Handb Exp Pharmacol* 184:171–206. https://doi.org/10.1007/978-3-540-74805-2_7
20. Duregotti E et al (2015) "Mitochondrial alarmins released by degenerating motor axon terminals activate perisynaptic Schwann cells," (in eng). *Proc Natl Acad Sci U S A* 112(5):E497–505. <https://doi.org/10.1073/pnas.1417108112>
21. Negro S et al (2017) CXCL12 α /SDF-1 from perisynaptic Schwann cells promotes regeneration of injured motor axon terminals. *EMBO Mol Med* 9(8):1000–1010. <https://doi.org/10.15252/emmm.201607257>
22. Rodella U et al (2016) "An animal model of miller fisher syndrome: mitochondrial hydrogen peroxide is produced by the autoimmune attack of nerve terminals and activates Schwann cells," (in eng). *Neurobiol Dis* 96:95–104. <https://doi.org/10.1016/j.nbd.2016.09.005>
23. Negro S et al (2018) "Hydrogen peroxide is a neuronal alarmin that triggers specific RNAs, lateral translation of Annexin A2, and cytoskeletal remodeling in Schwann cells," (in eng). *RNA* 24(7):915–925. <https://doi.org/10.1261/rna.064816.117>
24. Napoli I et al (2012) "A central role for the ERK-signaling pathway in controlling Schwann cell plasticity and peripheral nerve regeneration in vivo," (in eng). *Neuron* 73(4):729–742. <https://doi.org/10.1016/j.neuron.2011.11.031>
25. Malik AR, Liszewska E, Jaworski J (2015) "Matricellular proteins of the Cyr61/CTGF/NOV (CCN) family and the nervous system," (in eng). *Front Cell Neurosci* 9:237. <https://doi.org/10.3389/fncel.2015.00237>
26. Mallon BS, Shick HE, Kidd GJ, Macklin WB (2002) "Proteolipid promoter activity distinguishes two populations of NG2-positive cells throughout neonatal cortical development," (in eng). *J Neurosci* 22(3):876–885
27. Tosolini AP, Villarroel-Campos D, Schiavo G, Sleight JN (2021) "Expanding the toolkit for in vivo imaging of axonal transport," (in eng). *J Vis Exp*. <https://doi.org/10.3791/63471>
28. Rigoni M et al (2005) Equivalent effects of snake PLA2 neurotoxins and lysophospholipid-fatty acid mixtures. *Science* 310(5754):1678–1680. <https://doi.org/10.1126/science.1120640>
29. Rossetto O, Gorza L, Schiavo G, Schiavo N, Scheller RH, Montecucco C (1996) VAMP/synaptobrevin isoforms 1 and 2 are widely and differentially expressed in nonneuronal tissues. *J Cell Biol* 132(1–2):167–179. <https://doi.org/10.1083/jcb.132.1.167>
30. Antonucci F, Rossi C, Gianfranceschi L, Rossetto O, Caleo M (2008) "Long-distance retrograde effects of botulinum neurotoxin A," (in eng). *J Neurosci* 28(14):3689–3696. <https://doi.org/10.1523/JNEUROSCI.0375-08.2008>
31. Zanetti G et al (2017) "Botulinum neurotoxin C mutants reveal different effects of syntaxin or SNAP-25 proteolysis on neuromuscular transmission," (in eng). *PLoS Pathog* 13(8):e1006567. <https://doi.org/10.1371/journal.ppat.1006567>
32. Cox TF, Cox MAA (2001) *Multidimensional Scaling*, 2nd edn. Chapman and Hall, London
33. Robinson MD, McCarthy DJ, Smyth GK (2010) "edgeR: a Bioconductor package for differential expression analysis of digital gene expression data," (in eng). *Bioinformatics* 26(1):139–140. <https://doi.org/10.1093/bioinformatics/btp616>
34. Ikawa Y et al (2008) "Neutralizing monoclonal antibody to human connective tissue growth factor ameliorates transforming growth factor-beta-induced mouse fibrosis," (in eng). *J Cell Physiol* 216(3):680–687. <https://doi.org/10.1002/jcp.21449>
35. Sigounas G, Harindranath N, Donadel G, Notkins AL (1994) "Half-life of polyreactive antibodies," (in eng). *J Clin Immunol* 14(2):134–140. <https://doi.org/10.1007/BF01541346>
36. Dun XP, Parkinson DB (2018) "Transection and crush models of nerve injury to measure repair and remyelination in peripheral nerve," (in eng). *Methods Mol Biol* 1791:251–262. https://doi.org/10.1007/978-1-4939-7862-5_20
37. Zanetti G et al (2019) "A CXCR4 receptor agonist strongly stimulates axonal regeneration after damage," (in eng). *Ann Clin Transl Neurol*. <https://doi.org/10.1002/acn3.50926>
38. Sleight JN, Tosolini AP, Schiavo G (2020) "In vivo imaging of anterograde and retrograde axonal transport in rodent peripheral nerves," (in eng). *Methods Mol Biol* 2143:271–292. https://doi.org/10.1007/978-1-0716-0585-1_20
39. Stazi M et al (2021) "Melatonin promotes regeneration of injured motor axons via MT," (in eng). *J Pineal Res* 70(1):e12695. <https://doi.org/10.1111/jpi.12695>
40. Negro S, Stazi M, Rigoni M, Meghian A (2022) "Neurotransmission recovery by melatonin measured by CMAP," (in eng). *Methods Mol Biol* 2550:413–423. https://doi.org/10.1007/978-1-0716-2593-4_40
41. Dun XP, Parkinson DB (2018) "Whole mount immunostaining on mouse sciatic nerves to visualize events of peripheral nerve regeneration," (in eng). *Methods Mol Biol* 1739:339–348. https://doi.org/10.1007/978-1-4939-7649-2_22
42. Dickinson BC, Peltier J, Stone D, Schaffer DV, Chang CJ (2011) "Nox2 redox signaling maintains essential cell populations in the brain," (in eng). *Nat Chem Biol* 7(2):106–112. <https://doi.org/10.1038/nchembio.497>
43. Rigoni M et al (2007) Calcium influx and mitochondrial alterations at synapses exposed to snake neurotoxins or their phospholipid hydrolysis products. *J Biol Chem* 282(15):11238–11245. <https://doi.org/10.1074/jbc.M610176200>
44. Tang TT et al (2021) "Small molecule inhibitors of TEAD auto-palmitoylation selectively inhibit proliferation and tumor growth of," (in eng). *Mol Cancer Ther* 20(6):986–998. <https://doi.org/10.1158/1535-7163.MCT-20-0717>
45. Liang CC, Park AY, Guan JL (2007) "In vitro scratch assay: a convenient and inexpensive method for analysis of cell migration in vitro," (in eng). *Nat Protoc* 2(2):329–333. <https://doi.org/10.1038/nprot.2007.30>
46. Clements MP et al (2017) "The wound microenvironment reprograms schwann cells to invasive mesenchymal-like cells to drive peripheral nerve regeneration," (in eng). *Neuron* 96(1):98–114.e7. <https://doi.org/10.1016/j.neuron.2017.09.008>
47. Ojeda J et al (2020) "The Mouse," (in eng). *Front Cell Neurosci* 14:225. <https://doi.org/10.3389/fncel.2020.00225>
48. Negro S et al (2016) "ATP released by injured neurons activates schwann cells," (in eng). *Front Cell Neurosci* 10:134. <https://doi.org/10.3389/fncel.2016.00134>
49. Son YJ, Trachtenberg JT, Thompson WJ (1996) "Schwann cells induce and guide sprouting and reinnervation of neuromuscular junctions," (in eng). *Trends Neurosci* 19(7):280–285. [https://doi.org/10.1016/S0166-2236\(96\)10032-1](https://doi.org/10.1016/S0166-2236(96)10032-1)
50. Zhao B et al (2008) "TEAD mediates YAP-dependent gene induction and growth control," (in eng). *Genes Dev* 22(14):1962–1971. <https://doi.org/10.1101/gad.1664408>
51. Grove M, Lee H, Zhao H, Son YJ (2020) "Axon-dependent expression of YAP/TAZ mediates Schwann cell remyelination but not proliferation after nerve injury," (in eng). *Elife*. <https://doi.org/10.7554/eLife.50138>
52. Cicha I, Goppelt-Struebe M (2009) "Connective tissue growth factor: context-dependent functions and mechanisms of regulation," (in eng). *Biofactors* 35(2):200–208. <https://doi.org/10.1002/biof.30>
53. Mokalled MH, Patra C, Dickson AL, Endo T, Stainier DY, Poss KD (2016) "Injury-induced ctgfa directs glial bridging and spinal cord regeneration in zebrafish," (in eng). *Science* 354(6312):630–634. <https://doi.org/10.1126/science.aaf2679>
54. Hervera A et al (2018) "Reactive oxygen species regulate axonal regeneration through the release of exosomal NADPH oxidase 2 complexes into injured axons," (in eng). *Nat Cell Biol* 20(3):307–319. <https://doi.org/10.1038/s41556-018-0039-x>
55. Grotendorst GR, Duncan MR (2005) "Individual domains of connective tissue growth factor regulate fibroblast proliferation and myofibroblast

- differentiation," (in eng). *Faseb j* 19(7):729–738. <https://doi.org/10.1096/fj.04-3217com>
56. Gonzalez D et al (2018) "The inhibition of CTGF/CCN2 activity improves muscle and locomotor function in a murine ALS model," (in eng). *Hum Mol Genet* 27(16):2913–2926. <https://doi.org/10.1093/hmg/ddy204>
 57. Morales MG et al (2013) "Reducing CTGF/CCN2 slows down mdx muscle dystrophy and improves cell therapy," (in eng). *Hum Mol Genet* 22(24):4938–4951. <https://doi.org/10.1093/hmg/ddt352>
 58. Rebollo DL et al (2019) "Denervation-induced skeletal muscle fibrosis is mediated by CTGF/CCN2 independently of TGF- β ," (in eng). *Matrix Biol.* <https://doi.org/10.1016/j.matbio.2019.01.002>
 59. Lemaitre D et al (2020) "Collateral sprouting of peripheral sensory neurons exhibits a unique transcriptomic profile," (in eng). *Mol Neurobiol* 57(10):4232–4249. <https://doi.org/10.1007/s12035-020-01986-3>
 60. Chaqour B, Goppelt-Struebe M (2006) "Mechanical regulation of the Cyr61/CCN1 and CTGF/CCN2 proteins," (in eng). *FEBS J* 273(16):3639–3649. <https://doi.org/10.1111/j.1742-4658.2006.05360.x>
 61. Poitelon Y et al (2016) "YAP and TAZ control peripheral myelination and the expression of laminin receptors in Schwann cells," (in eng). *Nat Neurosci* 19(7):879–887. <https://doi.org/10.1038/nn.4316>
 62. Belin S, Zuloaga KL, Poitelon Y (2017) "Influence of mechanical stimuli on schwann cell biology," (in eng). *Front Cell Neurosci* 11:347. <https://doi.org/10.3389/fncel.2017.00347>
 63. Moya IM, Halder G (2019) "Hippo-YAP/TAZ signalling in organ regeneration and regenerative medicine," (in eng). *Nat Rev Mol Cell Biol* 20(4):211–226. <https://doi.org/10.1038/s41580-018-0086-y>

Publisher's Note

Springer Nature remains neutral with regard to jurisdictional claims in published maps and institutional affiliations.

Ready to submit your research? Choose BMC and benefit from:

- fast, convenient online submission
- thorough peer review by experienced researchers in your field
- rapid publication on acceptance
- support for research data, including large and complex data types
- gold Open Access which fosters wider collaboration and increased citations
- maximum visibility for your research: over 100M website views per year

At BMC, research is always in progress.

Learn more biomedcentral.com/submissions

